AD-A080 103 LOUISIANA STATE UNIV BATON ROUGE DIV OF ENGINEERING --ETC F/G 21/4
COMBUSTION KINETICS OF SELECTED AROMATIC HYDROCARBONS.(U)
AUG 79 R A MATULA, R C FARMER AFOSR-77-3384

UNCLASSIFIED AFOSR-TR-80-0077 NL

| OF |
AD
A080103

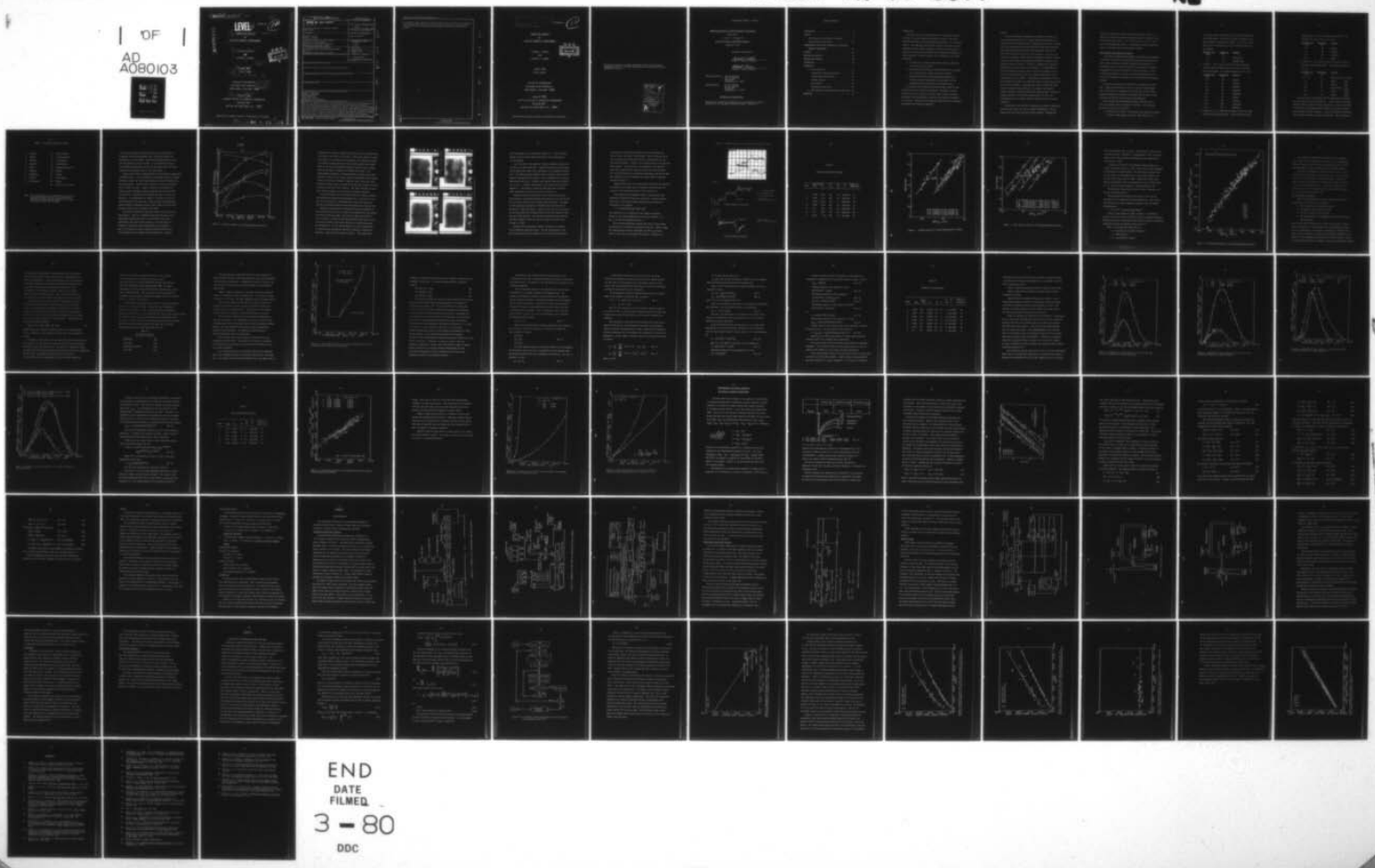

END
DATE
FILMED
3 - 80
DDC

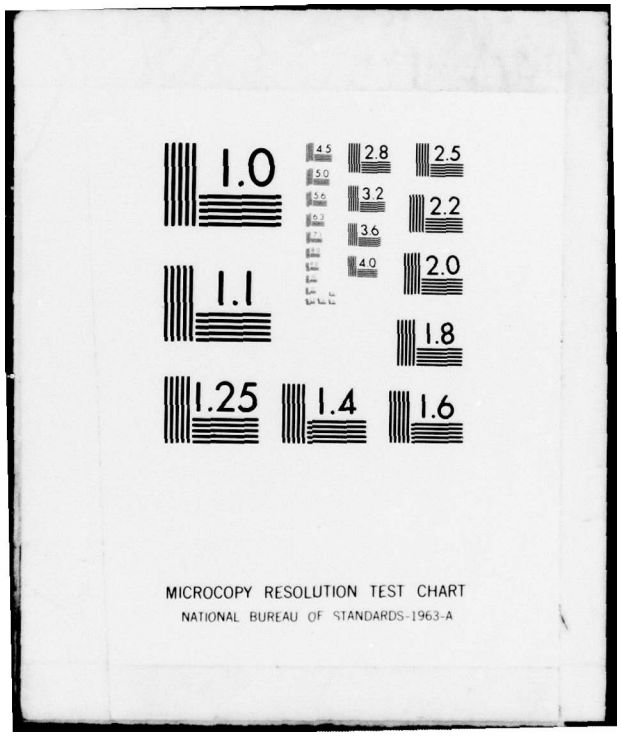
1.0
1.1
1.25
1.4
1.6
1.8
2.0
2.2
2.5
2.8
3.2
3.6
4.0
4.5
5.0
5.6
6.3
7.1
MICROCOPY RESOLUTION TEST CHART
NATIONAL BUREAU OF STANDARDS-1963-A

(18) AFOSR (19) TR-80-0077

AFOSR-TR- 80-0077

LEVEL II

(12)

AD A080103

AD59381

(6) COMBUSTION KINETICS OF SELECTED AROMATIC HYDROCARBONS.

(10) RICHARD A./MATULA AND RICHARD C./FARMER

(12) 85

(11) AUGUST 1979

(9) FINAL REPORT. / Jun 77-31 Aug 79

COLLEGE OF ENGINEERING
LOUISIANA STATE UNIVERSITY
BATON ROUGE, LOUISIANA 70803

(16) 2308

(17) B2

(15) ✓AFOSR-77-3384

AIRFORCE OFFICE OF SCIENTIFIC RESEARCH/NA
BUILDING 410
BOLLING AIR FORCE BASE, D.C. 20332

LB

REPORT DOCUMENTATION PAGE	READ INSTRUCTIONS BEFORE COMPLETING FORM
1. REPORT NUMBER: AFOSR-TR- 80-0077	2. GOVT ACCESSION NO. / 3. RECIPIENT'S CATALOG NUMBER
4. TITLE (and Subtitle): COMBUSTION KINETICS OF SELECTED AROMATIC HYDROCARBONS	5. TYPE OF REPORT & PERIOD COVERED: Final, 1 June 1977 - 31 August 1979
	6. PERFORMING ORG. REPORT NUMBER
7. AUTHOR(s): RICHARD A MATULA, RICHARD C FARMER	8. CONTRACT OR GRANT NUMBER(s): AFOSR 77-3384
9. PERFORMING ORGANIZATION NAME AND ADDRESS: LOUISIANA STATE UNIVERSITY, DIVISION OF ENGINEERING RESEARCH, BATON ROUGE, LOUISIANA 70803	10. PROGRAM ELEMENT, PROJECT, TASK AREA & WORK UNIT NUMBERS: 2308B2, 61102F
11. CONTROLLING OFFICE NAME AND ADDRESS: AIR FORCE OFFICE OF SCIENTIFIC RESEARCH/NA, BLDG 410, BOLLING AIR FORCE BASE, D C 20332	12. REPORT DATE: August 1979
	13. NUMBER OF PAGES: 82
14. MONITORING AGENCY NAME & ADDRESS(if different from Controlling Office)	15. SECURITY CLASS. (of this report): UNCLASSIFIED
	15a. DECLASSIFICATION/DOWNGRADING SCHEDULE

16. DISTRIBUTION STATEMENT (of this Report)

Approved for public release; distribution unlimited.

17. DISTRIBUTION STATEMENT (of the abstract entered in Block 20, if different from Report)

18. SUPPLEMENTARY NOTES

19. KEY WORDS (Continue on reverse side if necessary and identify by block number)

AROMATIC COMBUSION
AROMATIC PYROLYSIS
SOOT FORMATION
SHOCK TUBE STUDIES
SYNTHETIC FUEL COMBUSTION

20. ABSTRACT (Continue on reverse side if necessary and identify by block number)

The primary objective of the research program is to develop an understanding of the high temperature pyrolysis, oxidation and carbon formation processes in selected aromatic-hydrocarbon/air-combustion systems. The results of this study can be subsequently utilized to optimize the use of high-aromatic-content synthetic jet-fuels in both present and future jet combustors. Specific objectives of the research are to: study the kinetics of aromatic hydrocarbon pyrolysis in temperature and ranges of interest; study the ignition and oxidation of aromatic hydrocarbon-air systems; measure the critical fuel-oxidizer equivalence ratio

DD FORM 1 JAN 73 1473 EDITION OF 1 NOV 65 IS OBSOLETE

UNCLASSIFIED

SECURITY CLASSIFICATION OF THIS PAGE (When Data Entered)

for incipient soot formation in aromatic hydrocarbon-air mixtures; and develop quasi-global and/or detailed oxidation mechanisms for these aromatic hydrocarbons based on experimental data and computer modeling of the reaction systems.

AFOSR-TR-

COMBUSTION KINETCS
OF
SELECTED AROMATIC HYDROCARBONS

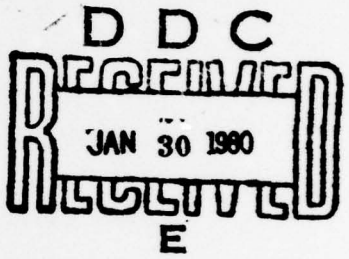

RICHARD A. MATULA

AND

RICHARD C. FARMER

AUGUST 1979

FINAL REPORT

COLLEGE OF ENGINEERING

LOUISIANA STATE UNIVERSITY

BATON ROUGE, LOUISIANA 70803

AFOSR-77-3384

AIR FORCE OFFICE OF SCIENTIFIC RESEARCH/NA

BUILDING 410

BOLLING AIR FORCE BASE, D.C. 20332

"Qualified requestors may obtain additional copies from the Defense Documentation Center, all others should apply to the National Technical Information Service".

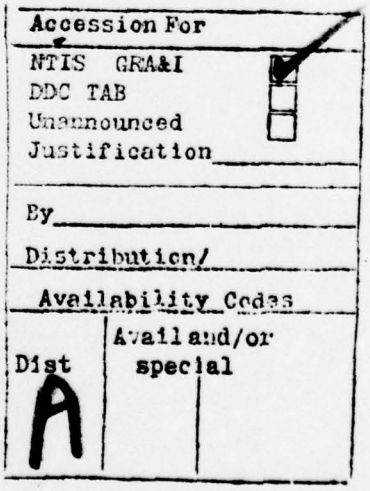

AFOSR REPORT NUMBER: AFOSR-TR-

COMBUSTION KINETICS OF SELECTED AROMATIC HYDROCARBONS

Final Report

1 June 77 - 31 August 79

Air Force Office of Scientific Research

August 31, 1979

Principal Investigators:

Richard A. Matula

Richard A. Matula, Professor

Richard C Farmer

Richard C. Farmer, Professor

Contracting Officer: Joan O. Marshall
PKD, Building 410
Bolling AFB
Washington, D.C. 20332

Program Manager: Dr. B.T. Wolfson
NA, Building 410
Bolling AFB
Washington, D.C. 20332

Conditions of Reproduction

TABLE OF CONTENTS

INTRODUCTION

The objective of this research study was to develop an understanding of the high temperature pyrolysis, oxidation and carbon formation processes in selected aromatic hydrocarbon - air combustion systems. The temperature and pressure ranges of interest are those encountered in jet turbine combustors, so that the results may be utilized to optimize the performance and minimize smoke formation in these combustors. Specific goals of this investigation are stated as follows:

1. The kinetics of aromatic hydrocarbon pyrolysis, ignition, and oxidation were studied.
2. The critical fuel/oxidizer equivalence-ratios for incipient soot formation with aromatic fuels were measured.
3. Quasi-global and/or detailed oxidation mechanisms for selected aromatic hydrocarbons were developed, so that experimental data could be more conveniently used.

The aromatic fuels considered during the study varied in ring structure and in the degree of saturation. The number of fuels studied were severely limited, and very little detailed mechanism development was accomplished, so that the study could be completed in two years. Otherwise, these goals were pursued with an integrated experimental and analytical approach.

RESULTS

The high temperature decomposition, ignition, oxidation, and soot forming characteristics of slected aromatic hydrocarbons was studied in both a conventional and a single-pulse shock tube. Results from these experiments have been modeled with quasi-global ignition delay expressions and with similar expressions that describe the delay time necessary for incipient soot formation. Most fuels are mixtures of compounds, rather than pure compounds, and since accurate kinetics models cannot be efficiently developed for mixtures, pure compounds only were studied. In order to understand the combustion and pyrolysis of pure, multi-atom compounds, it is advantageous to know how homologous compounds react. Toluene and benzene, the two most plentiful aromatics in both coal-syncrude distillates and unleaded gasoline, were studied. Cyclohexane, cyclopentane, iso-octane, and n-heptane were studied to obtain the effect of ring structure and of the ease of ignition. Ignition delay times for these fuel molecules were measured and reported(1). To expedite the study of aromatic behavior, toluene was chosen for detailed study. Benzene is equally important, but some data already exists for this fuel. Investigation of more complex aromatic compounds have not yet been considered.

The pyrolysis and oxidation of toluene were studied by measuring ignition delay times, the rate of toluene disappearance, and the composition of partially pyrolyzed toluene samples. Mathematical

models were devised to represent these observations. The rate at which soot formed from toluene was measured; the total amount of soot so formed was then computed. The delay time that it takes to form soot was mathematically modeled. A preliminary detailed mechanistic model to represent these observations was devised.

The Pyrolysis and Oxidation of Toluene

The chemical changes which accompany the pyrolysis and combustion of synthetic fuels may be qualitatively determined by measuring the stable species present in samples which have been quenched at an intermediate state of reaction and may be quantitatively determined by in situ spectroscopic measurements during experiments. Neither of these determinations is simple for large fuel molecules, but we believe that meaningful experiments can be performed by the following procedure.

The pyrolsis studies were carried out in a single-pulse shock-tube. Highly diluted mixtures of fuel in argon were shock heated over a wide variety of temperatures and pressures, and the stable quenched decomposition products were analyzed with the aid of flame ionization and thermal conductivity gas chromatographs.

Four different gas chromatograph columns, have been used to detect 19 products from the pyrolysis of toluene. In all columns, the carrier flow rate is 30 cc/min.

1. Molecular Sieve Column. Three columns are connected in series to make a total length of 21 feet. This column is used

to separate helium from hydrogen in the Thermal Conductivity Gas Chromatograph. The carrier is argon. Hydrogen is produced during the pyrolysis of toluene. Since helium is the driver gas in the shock tube, it will likely be present in the samples.

Retention Time (min)	Temperature (C)	Compound
4.0	20	Helium (He)
5.3	20	Hydrogen (H_2)

2. Porapak R. This column is used in the Flame Ionization Detector (FID) with helium carrier in order to separate C1-C4 hydrocarbons. The column dimensions are 9' x 1/8".

Retention Time (min)	Temperature (C)	Compound
0.6	60	Methane
1.5	60	Acetylene
1.75	60	Ethylene
7.05	60	Propylene
9.0	60	Propadiene
10.1	60	Propyne
15.2	90	Butylene
18.3	105	2-Butylene
21.7	105	Butadiene

3. Porapak R + R + Q. These three columns in series are used in the FID with helium carrier. This column separates C_2

hydrocarbons i.e., ethane, ethylene and acetylene. The dimensions for each column are 9' x 1/8".

Retention Time (min)	Temperature (C)	Compound
2.75	60	Methane
8.3	60	Ethylene
8.8	60	Acetylene
10.1	60	Ethane

4. Chromosorb W. This column is used in the FID in order to separate aromatic hydrocarbons. The column dimensions are 9' x 1/8".

Retention Time (min)	Temperature (C)	Compound	
0.9 - 2.0	70	Alkanes mixture (3 peaks)	
3.7	70	Benzene	C_6H_6
5.8	70	Toluene	C_7H_8
12.4	70	Ethyl Benzene	C_8H_{10}
15.5	70	Xylene	C_8H_{10}
24.7	70	Styrene	C_8H_8

Quenched samples are prepared with the single-pulse shock-tube and are analyzed by gas chromatography. Table I gives the products which have been detected in toluene analysis for a case in which 30% of the toluene was decomposed and one-third of the reacted toluene was recovered as gaseous fragments. Notice that some 18 species have been identified without using mass spectroscopy. This economic and

Table I. Pyrolysis Products of Toluene

1	Hydrogen	10	Cis-2-butylene
2	Methane	11	Trans-2-butylene
3	Ethylene	12	1,3-Butadiene
4	Acetylene	13	1,2-Butadiene
5	Ethane	14	Unidentified species
6	Propylene	15	Benzene
7	Propadiene	16	Toluene
8	Propene	17	Ethyl Benzene
9	Iso-butylene	18	Styrene
		19	Either m- or o-xylene

Note: 99 + % toluene was used to prepare the test mixtures. Toluene was found to be the only species present (besides the argon) when the unreacted test mixture was analyzed by gas chromatography.

time saving procedure was possible because of the high degree of technology in gas chromotography; slect calibration samples are available at very low prices. Multiple-ring compounds have not yet been identified, but soot is formed. It is believed that some of the multiple-ring compounds are lost on the system walls, but these compounds may be present only for very short times.

One percent toluene in argon mixtures were pyrolyzed at temperatures from 1200 to 1610 K. The concentrations of hydrogen, methane, ethylene, acetylene, benzene and toluene were measured in quenched samples from these experiments. Typical reaction times were 2 ms; the quenching rate was about 40 psi/ms. Figure 1 shows the concentrations of toluene, benzene, hydrogen, methane, ethylene, and acetylene which were measured. Increased shock strengths were used to control the pyrolysis. The compositions are shown as a function of reflected shock temperatures and pressures. Notice that the concentration of benzene reaches an apparent maximum at about 1450K, while all other pyrolized products are continuously increasing.

The measured toluene data show more scatter than that for the other species. This is a troublesome observation because several undesirable possibilities have to be considered before these concentration data may be fully utilized. Some toluene may be sticking to tube walls; small oxygen leaks may be consuming part of the toluene; or large, unstable precursor-molecules (to soot formation) may be forming and then decomposing. Repeated

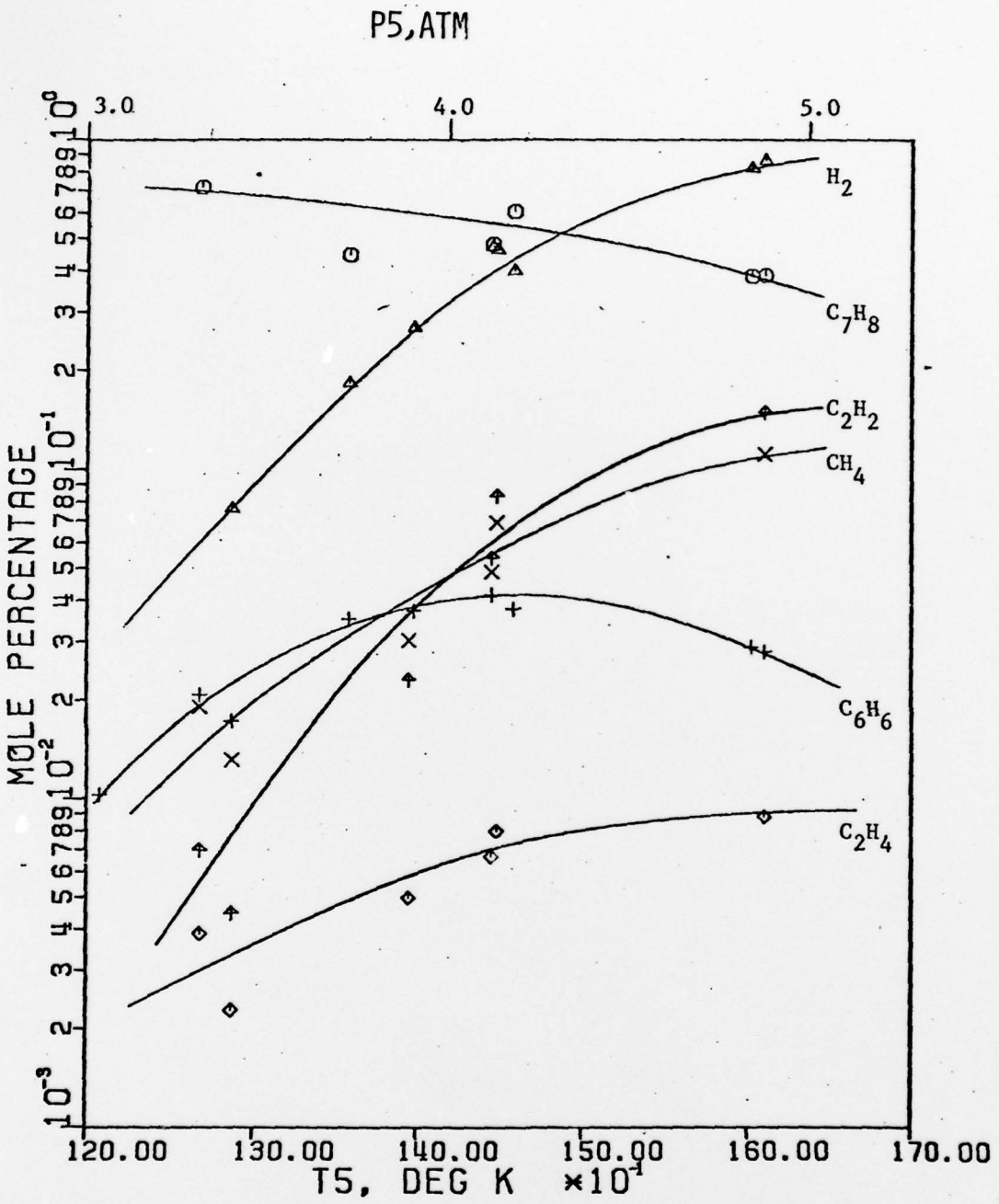

Figure 1. Pyrolysis Products of a Toluene/Oxygen/Argon Mixture.

measurements of test-gas composition indicate that low concentrations of toluene do not stick to tube walls. Oxygen leaks (which are large with respect to any which may be anticipated, but small with respect to creating an oxidizing mixture) have yielded quenched gas samples which do not show any measurable oxidation products; hence, oxygen leaks do not appear to explain the toluene data scatter. Gas chromotography techniques are being developed to measure multi-ring aromatics; therefore, the complex chemistry explanation of the toluene scatter will be made verifiable. Duplicate tests at the same shock conditions indicate that, even when the toluene data scatter, the other pyrolyzed product data do not scatter. The final conclusion is that these toluene fragments are the result of pyrolysis reactions.

Mass spectroscopic data have been reported for toluene pyrolysis and quenching in molecular beam experiments (2). These data are for only very low pressures. Measurements for large ionic species in benzene and acytelyne flames by mass spectroscopy are being made (3).

Moderately high resolution spectroscopy across the diameter of the shock-tube has been used to measure the composition of key species in toluene oxidation in situ. The spectral region from 2500 Å to 10 μ is studied. The most interesting observation was that at 3.35 μ C-H stretch radiation from toluene decreased as though the species was disappearing. For the same conditions, at 3.31 μ radiation due to temperature and composition indicates an increase in emitted IR radiation. Typical data are shown in Figure 2. The second worth-

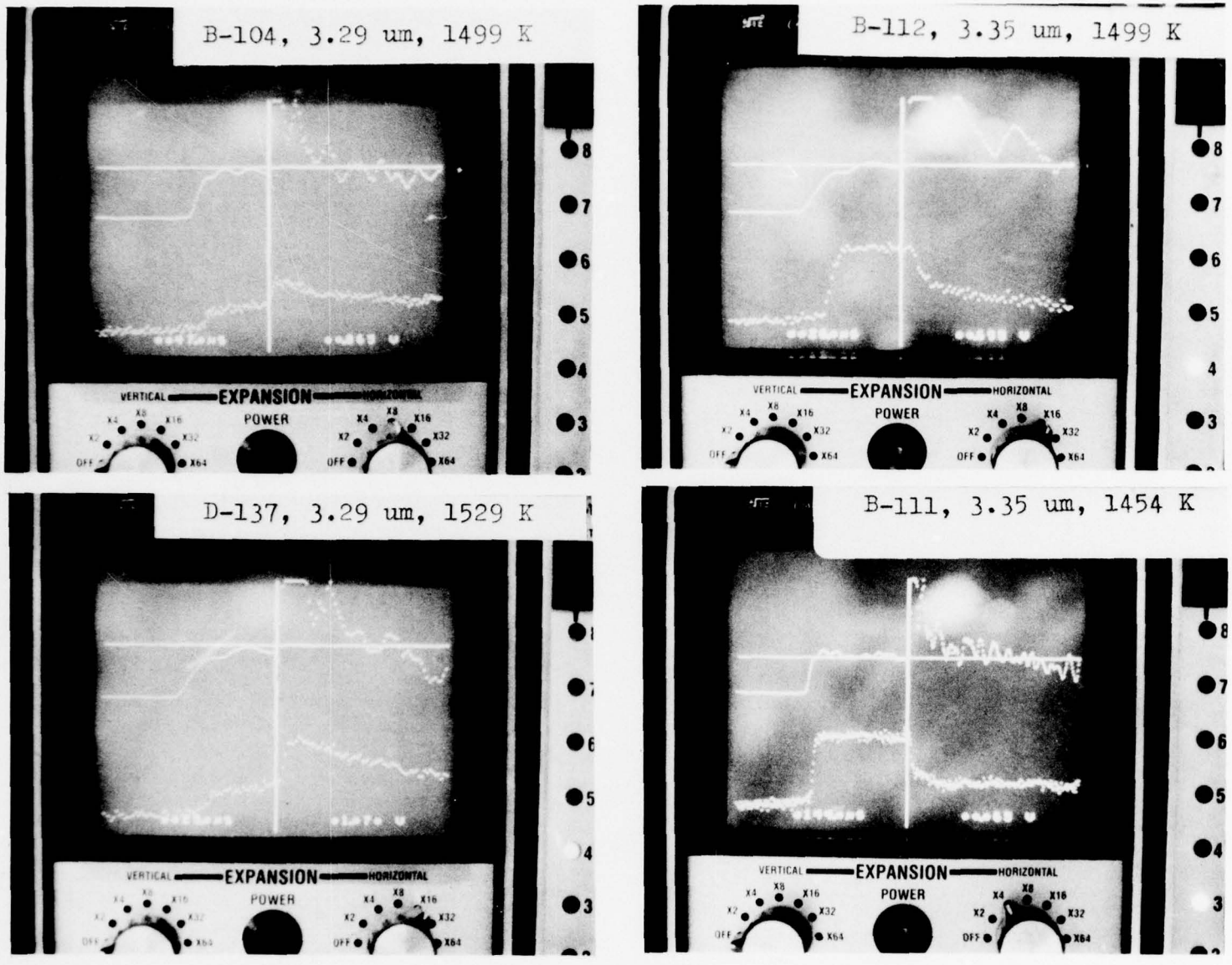

Figure 2. Infrared Radiation from Toluene/Oxygen/Argon Mixtures.

while measurement is of CO emission at about 5 μ. Other radiation appears to have so much mutual interference that interpretation is not feasible.

As in the case of the pyrolysis studies, oxidation studies were carried out in both shock tubes. Ignition delays have been measured in the single pulse shock tube, operating it as a conventional shock tube. The shock speed was measured with two Atlantic Research LD 25 pressure transducers and a counter. Both a DARCY/TSI and a Monsanto 100B counter were used. Incident shock traverse times were measured to $\pm$ 1 μsec. A complete description of this shock-tube is given in Appendix A. The method of converting shock speed into reflected shock temperature and pressure is shown in Appendix B.

Ignition delays were determined from a pressure measurement. The pressure of the ignition process was measured at the tube end and 5.3 cm from the tube end with a Kistler 603A transducer. The output of this gauge was displayed on a Tektronik 651A oscilloscope and recorded on a Polaroid picture. Ignition delay times were determined as the time between the reflected shock arrival and a departure from this post shock pressure. The accuracy of ignition delays obtained with the transducer in the end wall are judged to be within plus or minus 5 to 10%.

Ignition delay measurements depend, critically, on location of the combustion detection device. End cap measurements are the most accurate and show less dispersion than side wall measurements.

Corrections for side wall measurements can be established from the two sets of data which were obtained. These corrections can be used to compare our results with those of investigators who used side wall measurement. Figure 3 is a typical picture of the ignition delay studies. In this picture, the difference in the ignition delay times measured at the end and side wall is shown in detail. Due to this difference, our shock-tube measurements made on the side-wall resulted in an over estimation (by almost 100%) of apparent activation energies.

Ignition delay times for several hydrocarbon fuels were measured to establish the relative ease of combustion initiation and were reported in the 1978 Annual Report on this project (1).

Since pyrolysis and oxidation studies of benzene have been previously published(4) toluene was chosen for a detailed ignition delay study. The ignition delay measurements for toluene was correlated by the equation:

$$\tau = A\ (\exp(+E/RT))[C_7H_8]^a\ [O_2]^b\ [Ar]^c$$

The parameters to be evaluated were the apparent activation energy, E; the power dependencies of the three reactants, a, b, and c, and the pre-exponential factor, A.

Five toluene/oxygen/argon mixtures were used in seven groups of experiments to establish this empirical equation. Table II shows the concentrations and shock conditions for these experiments. Figure 4 and 5 show the individual data points. Mixtures A, B,

Figure 3. Typical Pressure Trace for the Ignition Delay Studies

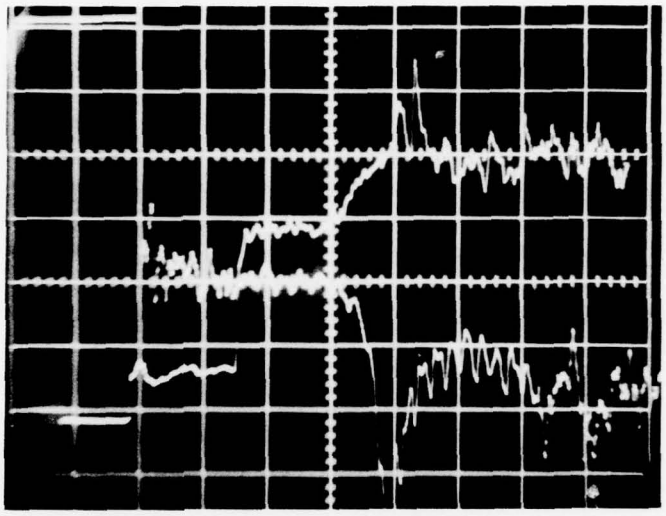

Where:

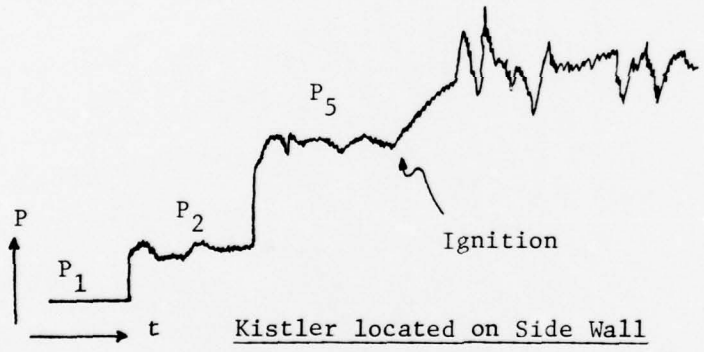

P_1 : Initial Pressure
P_2 : Incident Wave
P_5 : Reflected Wave
τsw: 180 μsec.
(Sweep = 100 μsec./div.)

Kistler located on Side Wall

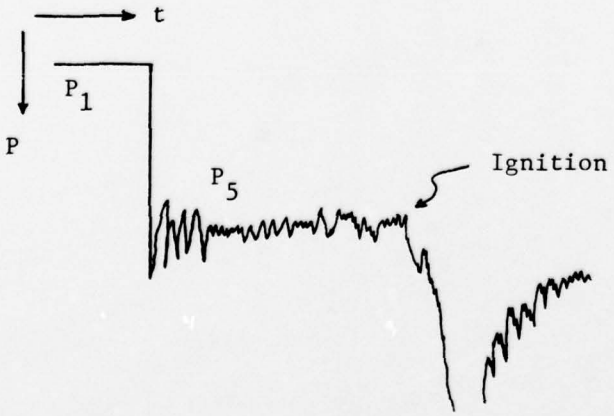

τew: 310 μsec.
(Sweep = 100 μsec./div.)

Kistler located at End Wall

Table II

Toluene Ignition-Delay Studies

Group	Mole Percent C_7H_8	Mole Percent O_2	P_1 torr	P_5 atm	T_5 K	Number of experiments
A	0.609	10.96	100	4.0	1272-1526	42
B	0.609	2.74	100	4.5	1528-1700	16
C	2.436	10.96	100	5.	1269-1397	19
D	0.609	5.48	225	9.7	1313-1616	17
E	2.0	18.0	100	4.5	1193-1362	20
F	2.0	18.0	50	2.5	1221-1441	26
G	0.609	5.48	100	4.2	1413-1643	18

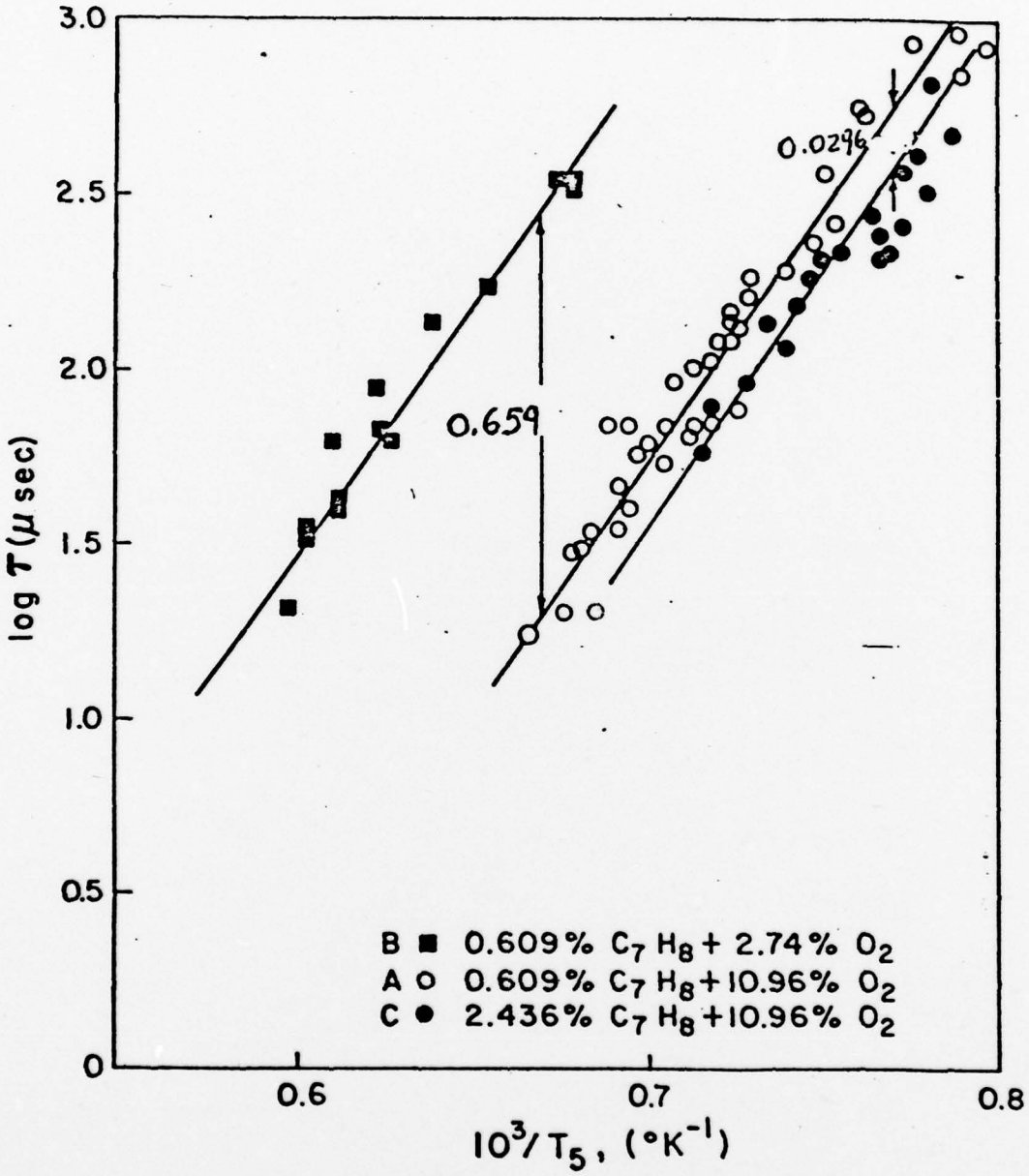

Figure 4 . Ignition Delays for Toluene/Oxygen/Argon Mixtures

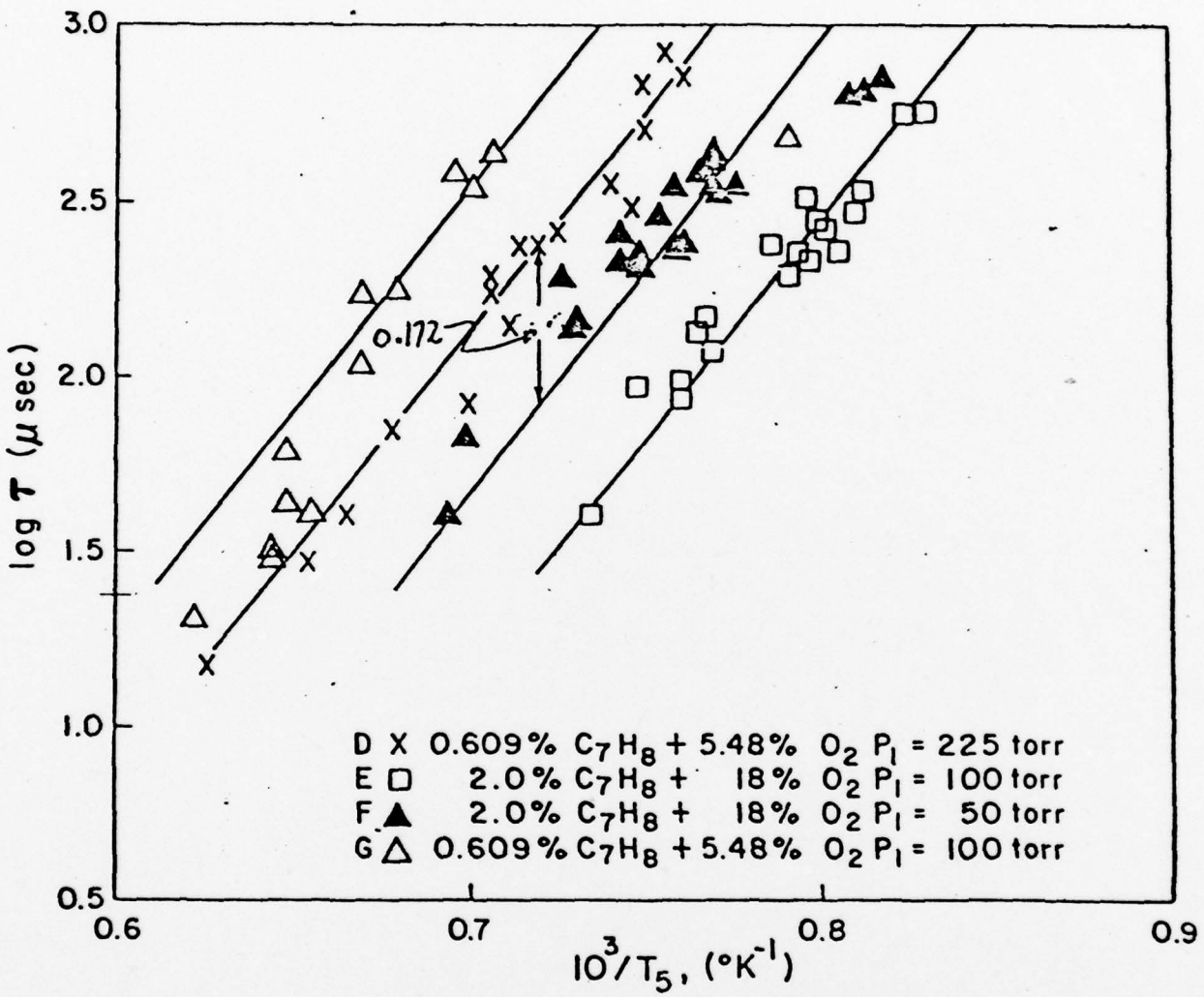

Figure 5. More Ignition Delays for Toluene/Oxygen/Argon Mixtures

and C are plotted as log τ vs $1/T_5$. The difference in log units on the graph is 0.659. Therefore b is approximately -1.09. Similarly, groups A and C will delineate the approximate power dependency of the fuel as a = 0.049

In Figure 5 the data for stoichiometric mixture groups D, E, F and G are plotted as log τ vs $1/T_5$. Here also the power dependence of the diluent is clearly defined. The fuel ratio in groups D and F is 3.28 and so is the oxygen ratio. The initial pressure ratio is 4.25, while the P_5 ratio is 2.986. Taking into account the Ar initial concentration ratio, the difference of the Ar concentration is 3.5. Thus, the power dependence c is approximately 0.516.

The difference between group E and F is only in pressure, the pressure difference being 2.

These approximate calculations are given to check correct correlation of the individual group experimentation. Final values were obtained via a linear regression analysis (after the proper transformations)

$$\tau = 3.0 \times 10^{-13} (\exp\{33/RT\})[O_2]^{-1}[Ar]^{0.5}$$

A plot of this equation is shown in Figure 6. Coefficients given in figure are those given directly from the regression analysis. Eliminating the fuel concentration term, because of lack of statistical significance yields the equation given in the text.

Where τ is the ignition delay time, sec

R = universal gas constant, kcal/mol.K

T = temperature, K

[ ] = concentration, moles/cc

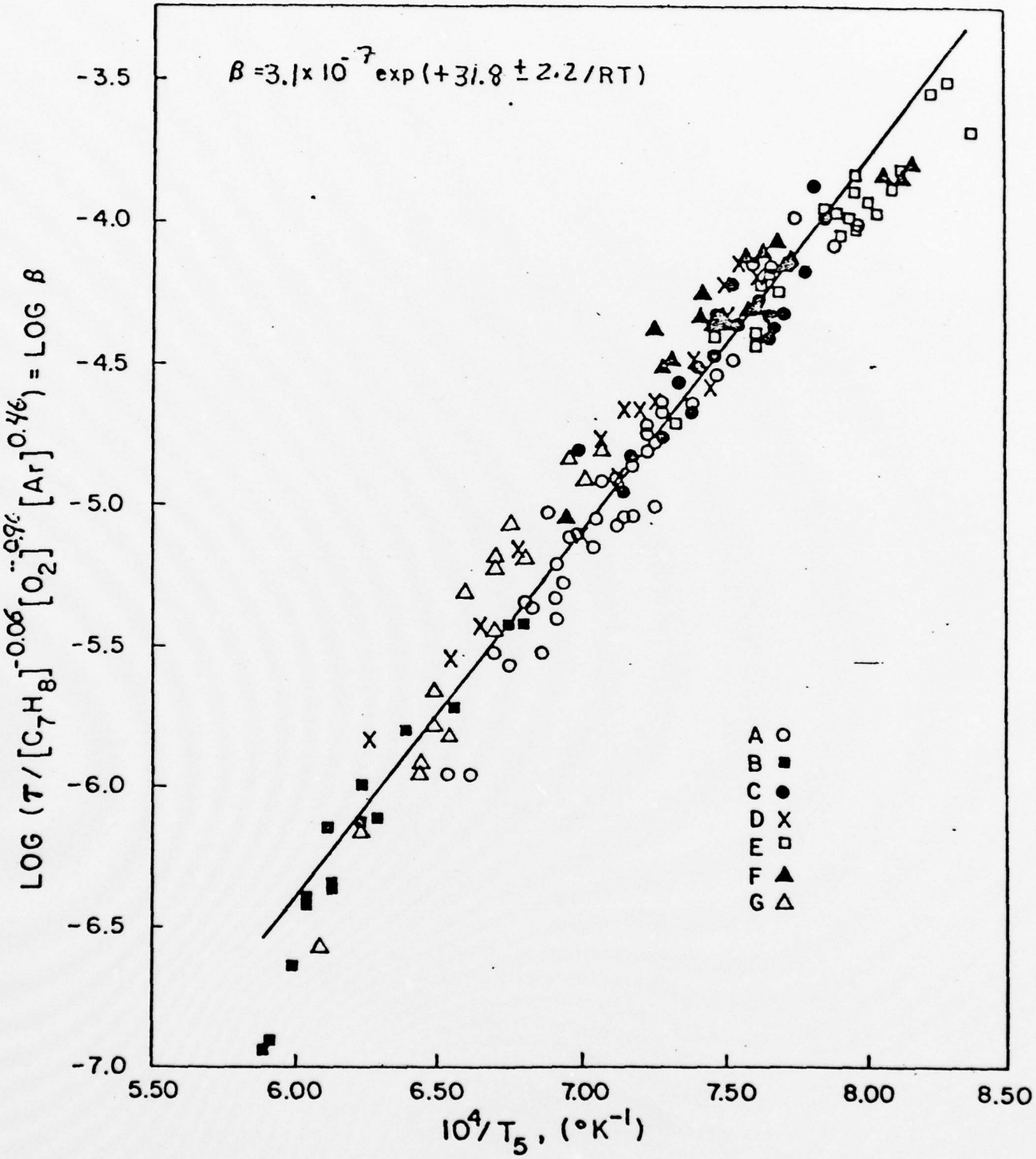

Figure 6 Correlation Equation for Toluene/Oxygen/Argon Mixtures

Two comparative ignition delay studies have been reported one of which is in air (5) and the other (6) is in an oxygen/argon mixture. Miyama (6) did not report a correlation equation with an argon dependency, so the equations cannot be directly compared.

The very low dependence on fuel and close to unity on oxygen concentration for initiation processes is not new since it has been found in a very large number of organic compounds. Usually this means that the fuel decomposes to radicals which react with oxygen in fast, chain-branching reactions. The positive dependence in argon however is not encountered with most small organic molecules, but is encountered with ethylene (7).

Soot Formation From Toluene

Shock-tube experiments can be used to generate four types of interesting data relative to soot formation.

1. The mixture ratios at which soot appears.
2. The amount of fuel converted to soot.
3. The time it takes for soot to form.
4. The identification of intermediate species which accompany soot production.

Many of these data already exist for simple fuel molecules. However, since the precursors to soot formation are large molecules and since soot is an agglomeration of molecules, mechanisms for formation rates have not been established. Neither the thermodynamic properties nor the identity of many important precursors have yet been determined. Hence, the sooting characteristics of synthetic fuels may be efficiently studied

by measuring and correlating the aforementioned data for pertinent fuel molecules, which include aromatics with various branches and degrees of aromaticity. Hypothesized precursors and soot structures will allow estimation of essential thermodynamic and kinetics data such that mechanisms may be postulated and compared to these correlations. The behavior of benzene, toluene, and acetylene should be firmly established first. Next, mixtures of these basic fuel molecules, and then multiple-ring compounds should be studied.

Measurements of the critical carbon to oxygen atom ratios for incipient soot formation were required because many investigators (8-17) have agreed that soot formation is a kinetically controlled process, since equilibrium calculations indicate that solid carbon should not be present at fuel-air mixture conditions where the carbon to oxygen atom ratio (C/O), $\emptyset$, is less than unity. They believe that the general chemical equation:

$$C_m H_n + X\ O_2 \rightarrow 2XCO + \frac{n}{2} H_2 + (\frac{m}{2} - X)C_s \qquad (1)$$

should efine a soot formation threshold, with no soot formation when $m < 2X$. Therefore, at any temperature when $\emptyset < \emptyset_c$, no soot should be formed.

Furthermore, there exists an upper temperature limit above which soot will not form. On the other hand, there also exists a lower temperature limit below which soot will not form. An increase of temperature shifts the upper limit C/O ratio to higher values, whereas a decrease in temperature has the effect of reducing the ability of fuel to form soot.
In other words, when the temperature is below the lower temperature

limit, the fuel remains unreacted in the test time available. As the temperature is increased, the present results show that the rate of soot formation and the soot yield increase until the temperature reaches approximately 1700K. At higher temperatures, the soot yield decreases until it becomes zero at the upper temperature limit. The fuel ceases to form soot because it decomposes to small gaseous hydrocarbon fragments and does not dehydrogenate or polymerize to form soot.

Experimentally determined critical carbon to oxygen atom ratios, however, do not occur at the $\phi_c = 1$ predicted from thermodynamic equilibrium calculations. Three different methods, utilizing the Bunsen burner flame (13), a flat flame (18) and a well stirred reactor (19,20) give similar results for ϕ_c, approximately 0.5 for hydrocarbon fuels in general. Pressure has very little effect on these values (11,17,21). Table III shows the results obtained from shock tube, flat flame and well-stirred reactor tests with toluene as fuel.

Table III

ϕ_c Values for Toluene

Experiment	ϕ_c
shock tube	0.85
well-stirred reactor	0.59
flat flame	0.52

The upper and lower temperature limits for soot formation at a given $\emptyset$ were determined by performing experiments at constant concentration and various temperatures. Temperature was varied to produce soot and no soot results until the critical temperature was determined to within $\pm$ 20K.

Figure 7 shows the variation of the upper and lower temperature limits as a function of carbon to oxygen ratio. The pressure of these tests was 5.0 $\pm$ 0.1 atm. The upper temperature limit, increases with $\emptyset$.

The results in Table III show that less oxygen is required to suppress the formation of carbon in the shock tube than in the jet-stirred reactor or a premixed flame. The $\emptyset_c$ value of 0.85 obtained from the shock tube is closer to unity then the other two values.

The difference is believed to be caused by the homogeneity of reactant gas mixtures. The homogeneity of the mixture used in shock tube experiments may be far greater than the other experimental methods. However, the large variation in duration of these experiments may explain this $\emptyset_c$ difference. The shock-tube experiments gave a maximum observation time of 4 milliseconds.

The shock-tube value of $\emptyset_c$ is still 0.15 different from the equilibrium value of unity. The question still exists as to whether this observation really supports the view that the formation of soot is a kinetic phenomena.

It is reported that soot, CO_2 and H_2O coexist in the combustion gases (17), although according to equilibrium calculations, they should not. This implies that the critical condition that every oxygen atom is

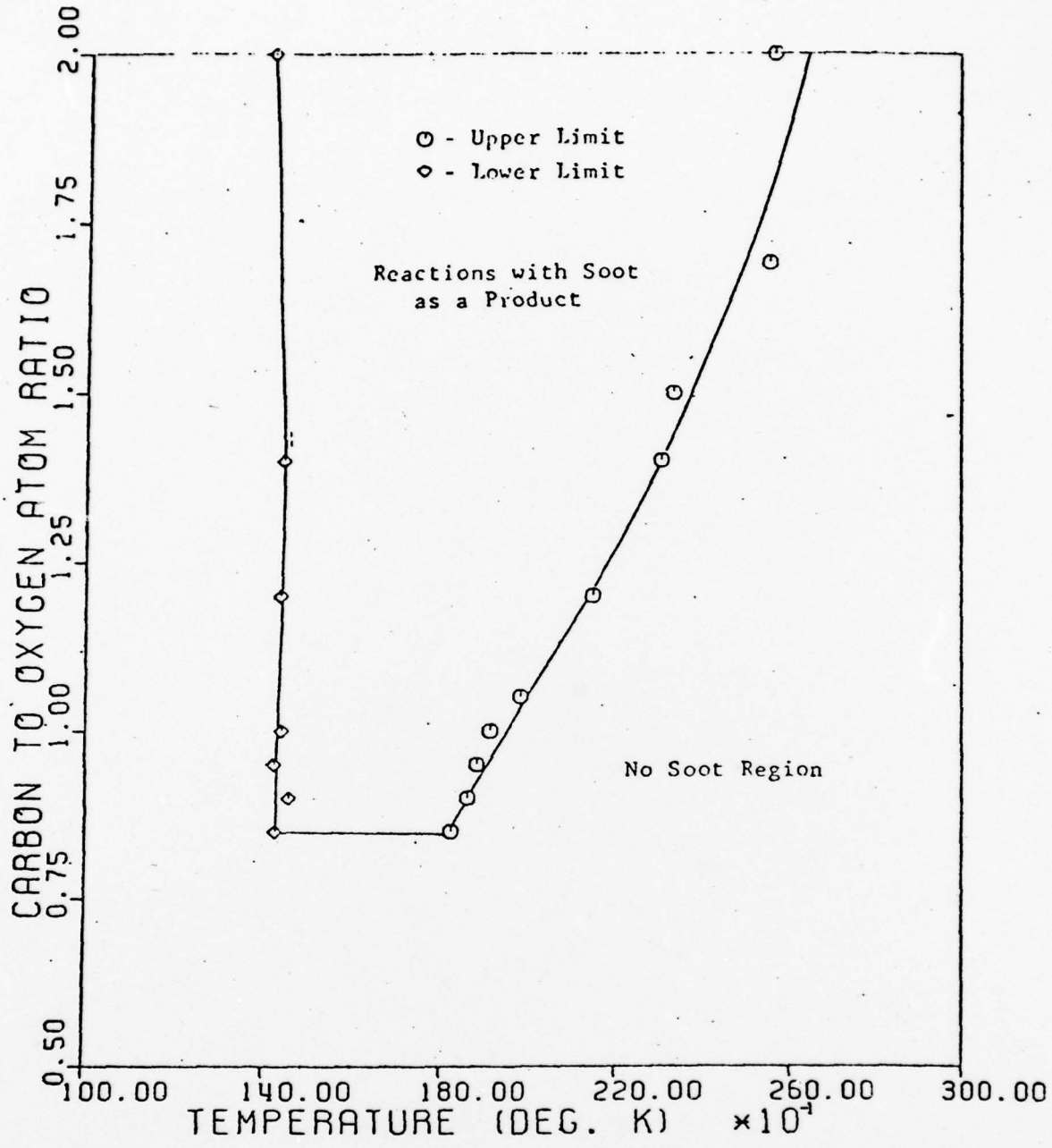

Figure 7. Soot Formation Limits in Toluene/Oxygen/Argon Mixtures at a Reflected Pressure of 5 Atmosphere

attached to a carbon atom has not been met. Therefore, carbon atoms are available to form soot. A schematic mechanism (9,17) is shown as follows:

$$RH + OH \longrightarrow R\cdot + H_2O \qquad (2)$$

$$CO + OH \rightleftarrows H + CO_2 \qquad (3)$$

$$H_2 + OH \rightleftarrows H + H_2O \qquad (4)$$

The reverse reactions of reaction (3) and reaction (4) which reduce H_2O and CO_2 have rather high activation energies of 86 kj/mol and 108 kj/mol respectively (22). This explains why part of the oxygen is not accessible in the time available during combustion processes. It is, therefore, probably reaction kinetics which is responsible for the appearance of soot at C/O ratios less than unity. The conclusion that soot is a kinetic phenomenon should not be drawn too quickly. If one examines the thermodynamic equilibrium calculations, it is found that there are no thermochemical properties of any polycyclic aromatic hydrocarbons, which are very important intermediates or final stable products, in the thermochemical library of the program. The lack of these thermochemical properties may produce significant errors in the calculations. Therefore, we cannot be definite about the validity of equilibrium results until the predictive scheme of thermochemical properties of polycyclic aromatic hydrocarbons has been successfully implemented, the data installed in the library, and subsequent equilibrium calculations conducted.

The amount of soot formed cannot be directly measured, but a calculation based upon a radiation absorption experiment can determine the amount formed. The details of this calculation are summarized in the following paragraphs.

The free and bound charges of any material are set into forced oscillation by an incident, periodic electromagnetic wave. The incident electromagnetic energy is partly scattered by the material, partly transmitted through it, and partily absorbed by the dissipative process within the material. Therefore, the total cross section for the particle comprises energy abstracted from the incident beam both by scattering and absorption. This is designated as the extinction cross section, C_e, and it is sum of the scattering cross section and the absorption cross section.

$$C_e = C_s + C_a \qquad \text{(Eq. 1)}$$

Most of the particles have an obvious geometrical cross section, A. Thus efficiency factors for extinction, scattering and absorption can be defined as follows:

$$\begin{aligned} Q_e &= C_e/A_e \\ Q_s &= C_s/A_s \\ Q_a &= C_a/A_a \end{aligned} \qquad \text{(Eq. 2)}$$

For quite general particles these factors depend on the orientation of the particle and on the state of polarization of the incident light. For spherical particles they are independent of both and $A_e = A_s = A_a = A$. Therefore, we have

$$Q_e = Q_s + Q_a \qquad \text{(Eq. 3)}$$

In other words, one can say Q_a is the ratio of the energy absorbed and converted into heat per unit time to the energy incident per unit time on the projected area of the sphere, while Q_e is the ratio of the energy absorbed and scattered per unit time to the energy incident on the projected area of the sphere.

The monochromatic emissivity observed along the path of length, L, which is the diameter of the shock tube is given as

$$E_\lambda = 1 - (1 - Q_s/Q_e) \exp \{- K_\lambda f_v \overline{C} L\} \qquad \text{(Eq. 4)}$$

$$= 1 - \left(I\{t\} / I\{0\}\right)$$

Where $\overline{C}$ is the density of hot soot particles, usually assumed to be 1.86 g/cm^3 (23), f_v is the volume fraction of space in the shock tube occupied by the soot particle and K_λ is the spectral attenuation coefficient.

The calculation of extinction and scattering efficiencies from a cloud of particles was first formulated by Mie (24), who developed a theroy of particle attenuation from a study of Maxwell's wave equations and give expressions for the extinction and scattering, in terms of the parameter X, and the complex refractive index m of the particle material as follows:

$$Q_e = \frac{1}{X^2} \sum_{n=1}^{\infty} (2n + 1) \text{ Re } \left\{a_n + b_n\right\} \qquad \text{(Eq. 5)}$$

$$Q_s = \frac{2}{X^2} \sum_{n=1}^{\infty} (2n + 1) \left(|a_n|^2 + |b_n|^2 \right) \qquad \text{(Eq. 6)}$$

where $X = \pi d/\lambda$.

Re {} means the real part of {},

a_n and b_n are the Mie coefficients, defined in terms of complex spherical Bessel Functions and their derivatives (25).

When $X < 0.5$, the Mie series are readily convergent and can be simplified to (26):

$$Q_e = \text{Im} \{-4X(m^2-1)/(m^2+2)\} \quad \text{(Eq. 7)}$$

$$Q_s = (8/3)X^4 \left|(m^2-1)/(m^2+2)\right|^2 \quad \text{(Eq. 8)}$$

where Im {} is the imaginary part of {}.

Since the scattering is calculated to be negligible compared with the absorption, the scattering efficiency can be neglected.

$$E_\lambda = 1 - \exp\{-K_\lambda f_v \bar{C} L\} \quad \text{(Eq. 9)}$$

Therefore, the attenuation of the incident laser light will be assumed to be completely caused by absorption, i.e., K_λ is now the spectral absorption coefficient.

Since the diameter of the soot particle, d, is so small (less than 300 Å), the spectral absorption coefficient can be calculated from the small particle limit of the Mie theory. It is therefore given by

$$K_\lambda = N(\pi/4)d^2 Q_e = N(\pi/4)d^2 Q_a \quad \text{(Eq. 10)}$$

Where N is the number of particles per unit weight (gm).

$$N = ((4\pi r^3/3)\bar{C})^{-1} = 6/\pi d^3 \bar{C} \quad \text{(Eq. 11)}$$

Substitute equation (9) into equation (8), we have

$$K_\lambda = (3/2)(Q_a/d\bar{C}) \quad \text{(Eq. 12)}$$

Assume the particle volume of hydrogen in a soot particle is negligible in comparison with the particle volume of carbon. We have

$$C_{soot} = N_o \bar{C} f_v / 12 \qquad \text{(Eq. 13)}$$

Combining equation 4 and equation 9, we get

$$\ln(I\{t\}/I\{0\}) = -K_\lambda f_v \bar{C} L \qquad \text{(Eq. 14)}$$

Substituting equation 12 into equation 14

$$\ln (I\{t\}/I\{0\}) = (-3/2)(f_v Q_a L/d) \qquad \text{(Eq. 15)}$$

$$\text{Let } E\{m\} = -Im\{(m^2-1)/(m^2+2)\} \qquad \text{(Eq. 16)}$$

Substituting equation 7 into equation 15, yields

$$\ln\{I\{t\}/I\{0\}\} = 6\pi L f_v E\{m\}/\lambda \qquad \text{(Eq. 17)}$$

or,

$$f_v = \ln\{I\{t\}/I\{0\}\}\ \lambda/6\pi L E\{m\} \qquad \text{(Eq. 18)}$$

Substituting equation 18 into equation 13, yields

$$C_{soot} = (N_o \bar{C}\lambda/72\pi L E\{m\}) \ln\{I\{0\}/I\{t\}\} \qquad \text{(Eq. 19)}$$

Further assume all the observed laser beam attenuation is caused by soot particles. The soot yield y will be given by

$$y = C_{soot}/C_5 = (N_o \bar{C}\lambda/72\pi L E\{m\} C_5) \ln\{I\{0\}/I\{t\}\} \qquad \text{(Eq. 20)}$$

where C_5 is the total concentration of carbon atoms behind the reflected shock wave, assuming frozen composition.

Soot yield studies using this analysis are presented in subsequent paragraphs. Note should be made that this analysis over estimates the amount of soot formed, yet the results are still interesting.

Seven toluene-oxygen mixtures were used in five groups of experiments to carry out the soot yield studies. Table IV shows the concentrations and shock conditions for these experiments. 2.5 ms after the shockwave

Table IV

Toluene Soot Yield Studies

Group	Mole % C_7H_8	C_2H_2	O_2	H_2	Ø	P_5 atm	T_5 K	Number of Experiments
A	0.300	0.0	0.8750	0.0	1.2	5	1438-1990	29
B	0.300	0.0	0.2100	0.0	5	5	1437-2260	36
C	0.600	0.0	0.3500	0.0	6	2.5	1338-2510	29
D	0.200	0.0	0.3500	0.0	2	2.5	1453-2008	22
E	0.150	0.0	0.0875	0.0	6	10	1369-2183	30
F	0.157	0.5	0.8750	0.0	1.2	5	1465-1843	29
G	0.3	0.0	0.8750	0.3	1.2	5	1425-1980	19

reflected from the end cap was taken as the time for comparison since it precedes the arrival of the expansion wave, and usually it was the time of maximum soot yield.

Figure 8 shows the suppression effect of oxygen on soot yields.

Figure 9 shows that an increase of toluene partial pressure increases soot yields.

Figure 10 shows the pressure effect on soot yields. A very interesting phenomena is observed at temperatures below 1700 K which is usually the temperature where we have maximum soot yield. The increase of pressure increases the soot yields, while above 1700 K, the increase of pressure decreases the soot yields.

Figure 11 indicates the mechanism of soot formation. Fragmentation is not a major soot producing step, since the soot yield is apparently depressed when half of the carbon atoms in the toluene are replaced by carbon atoms from acetylene. On the other hand, adding hydrogen does not reduce soot yields. Since dehydrogenation is an important step in soot formation, the extra hydrogen should retard this process. This matter warrents further investigation. Probably, more hydrogen would show the expected effect, because 3.5 to 12 moles of hydrogen per mole of napthene are used to prevent coke formation during catalytic reforming operations (27).

All the figures show the soot yield is zero at the lower temperature limit, then it increases with temperature to a maximum yield, before it decreases with temperature until the upper temperature limit is reached.

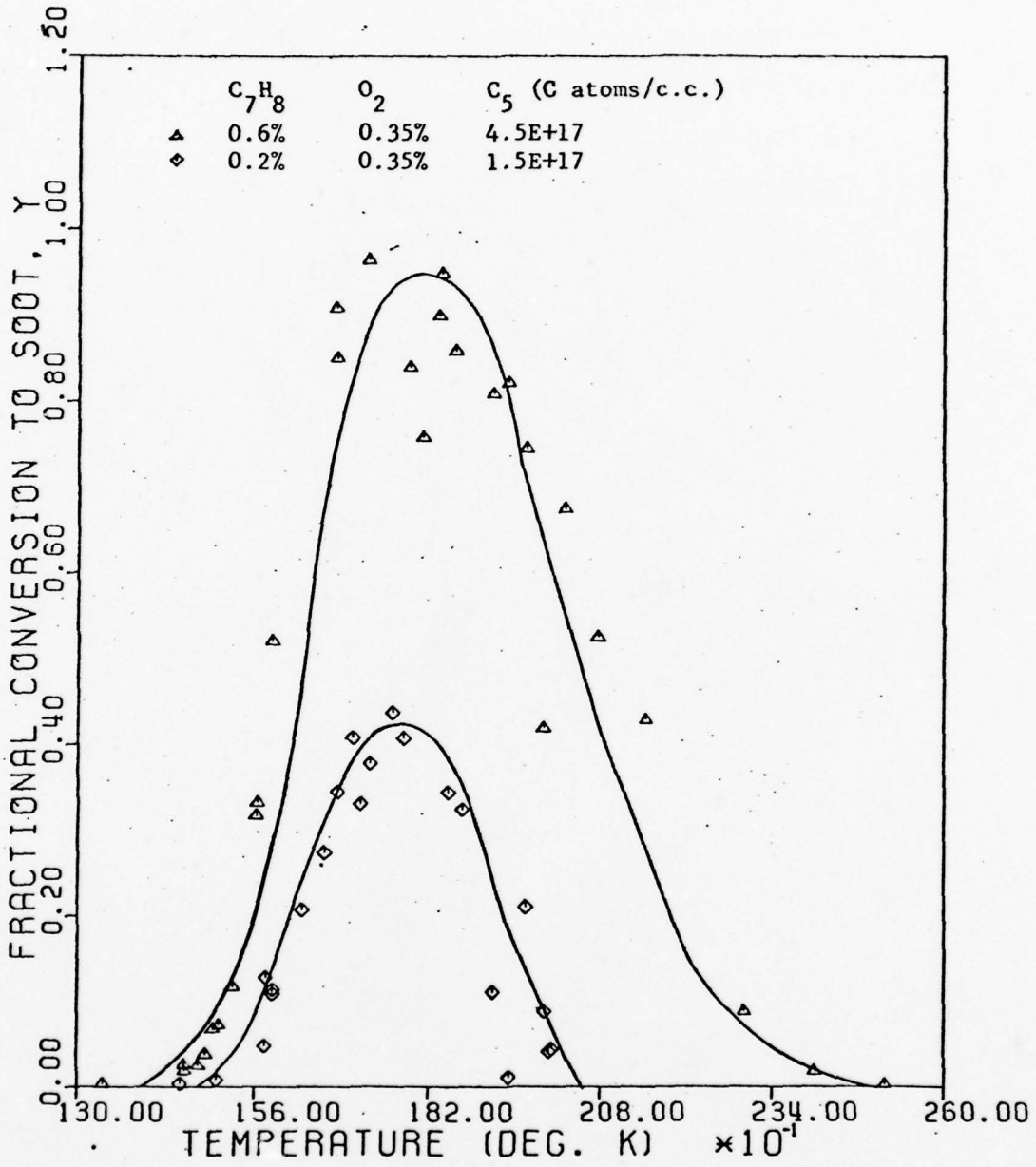

Figure 8. Comparison of soot yields at 2.5 ms after the onset of reflected shocks for toluene dependency.

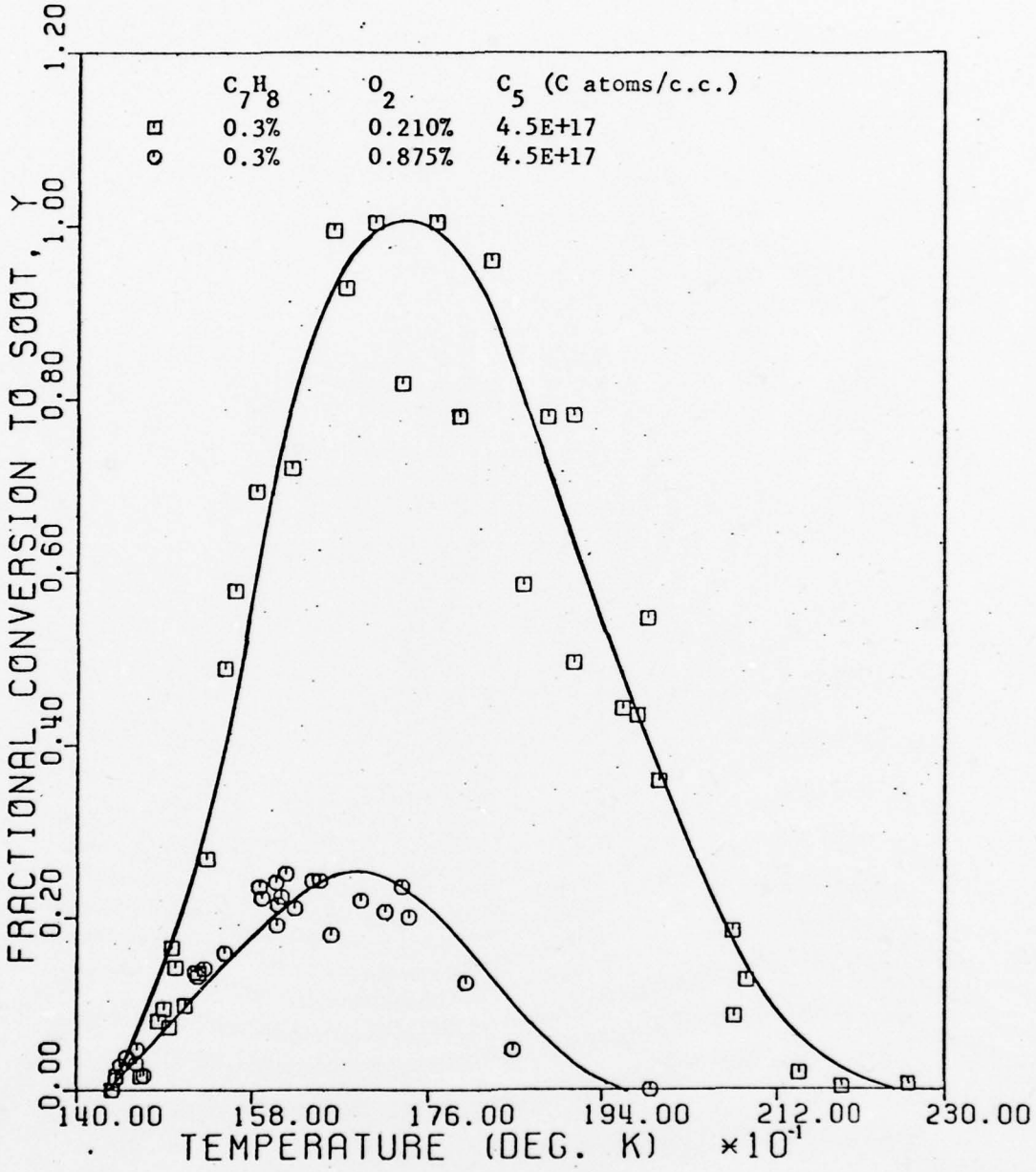

Figure 9. Comparison of soot yields at 2.5 ms after the onset of reflected shocks for oxygen dependency.

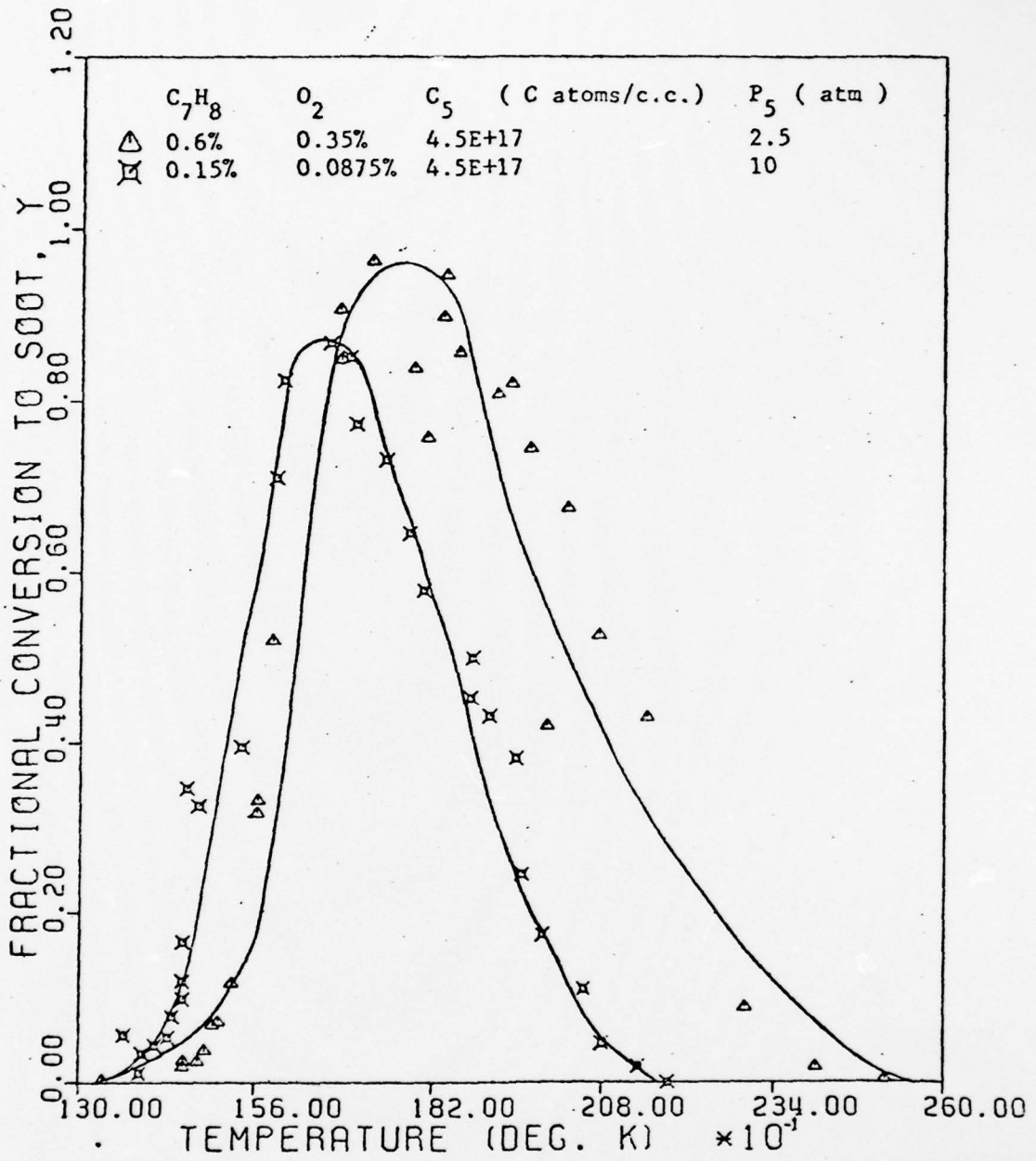

Figure 10. Comparison of soot yields at 2.5 ms after the onset of reflected shocks for argon dependency.

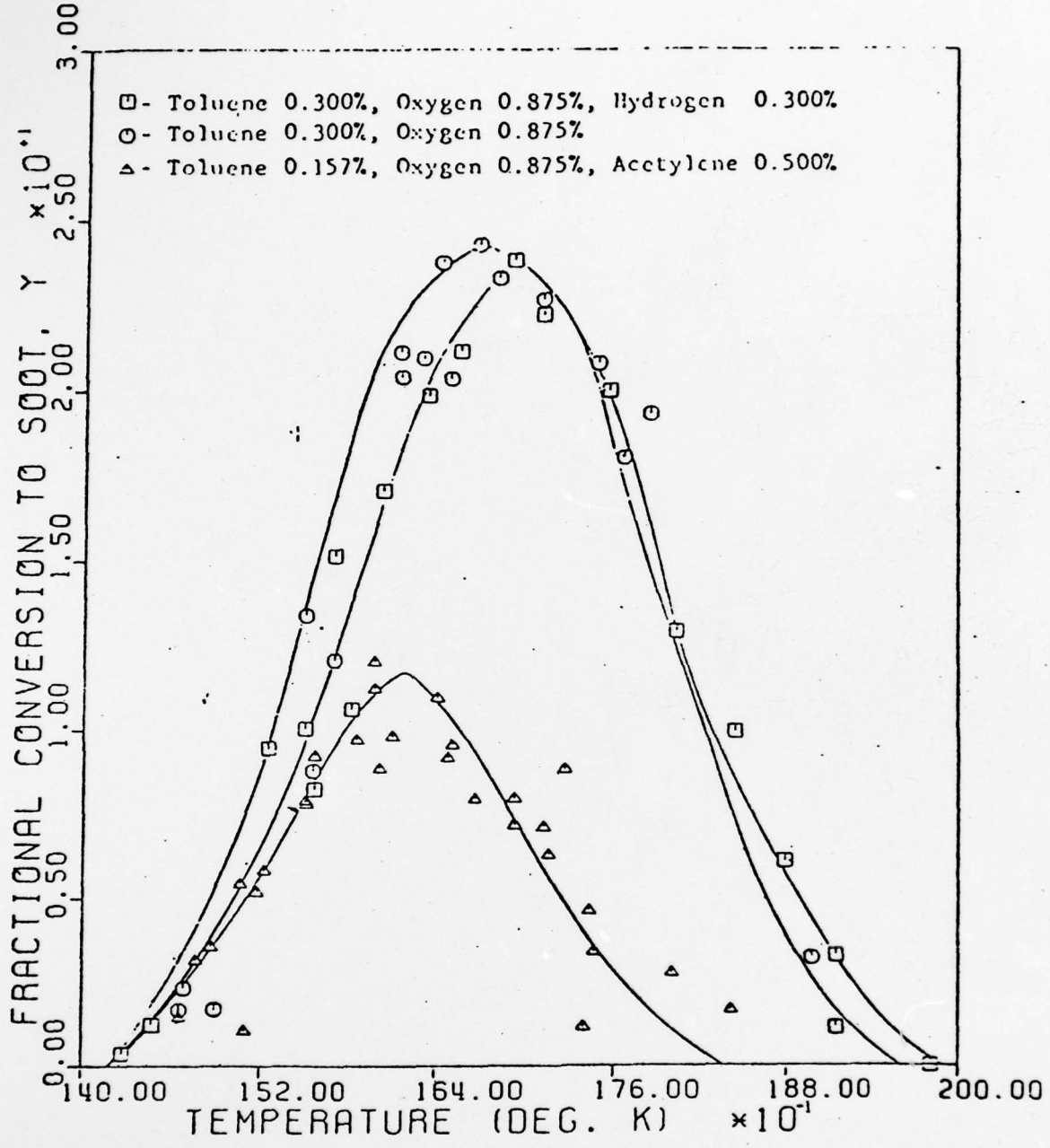

Figure 11. Comparison of Soot Yield at 2.5 ms after the Onset of Reflected Shocks

During the course of the soot formation experiments, an induction period ranging from approximately 20 to 2500 μsec was observed before any absorption occured. This period was defined as the soot formation delay time, τ_{soot}. It is interpreted as the time required for the fragmentation or condensation process to form soot. Therefore, it is postulated that the measurement and correlation of the soot formation delay time can be a useful tool in studying the kinetics of sooting. The following empirical formula for correlating delay time was utilized.

$$\tau_{soot} = A \exp(+E/RT)(C_7H_8)^a(O_2)^b(Ar)^c \qquad \text{(Eq. 21)}$$

Five toluene/oxygen/argon mixtures were used in three groups of experiments to establish this empirical equation. Table V shows the concentrations and shock conditions for these experiments.

Final values were estimated with a linear regression analysis using a logarithmic form of (Eq. 21).

$$\tau(\mu sec) = 1.4*10^{-16}(\exp(64.0\pm3.7/RT))(C_7H_8)^{-1.91\pm0.19}$$
$$*(O_2)^{0.78\pm0.12}(Ar)^{-0.36\pm0.17} \qquad \text{(Eq. 22)}$$

Figure 12 is a presentation of log α vs $1/T_5$ for the power dependencies found, where

$$\alpha = \tau_{soot}/A(C_7H_8)^a(O_2)^b(Ar)^c \qquad \text{(Eq. 23)}$$

The solid line represents the correlation equation.

The value of -1.91 for toluene dependency shows the soot forms earlier as toluene partial pressure increases. The value of +0.78 for oxygen dependency shows the soot forms slower as oxygen pressure increases, i.e., the representation of the suppressing effect by

Table V

Soot Formation Delay Studies

Group	C_7H_8	O_2	Ø	P_5 atm	T_5 K	Number of Experiments
H	0.3	0.875	1.2	5	1446-1916	38
I	0.3	0.210	5	5	1442-1787	34
J	0.2	0.350	2	2.5	1491-1997	50
K	0.6	0.350	6	2.5	1458-1840	34
L	0.15	0.0875	6	10	1398-1706	30

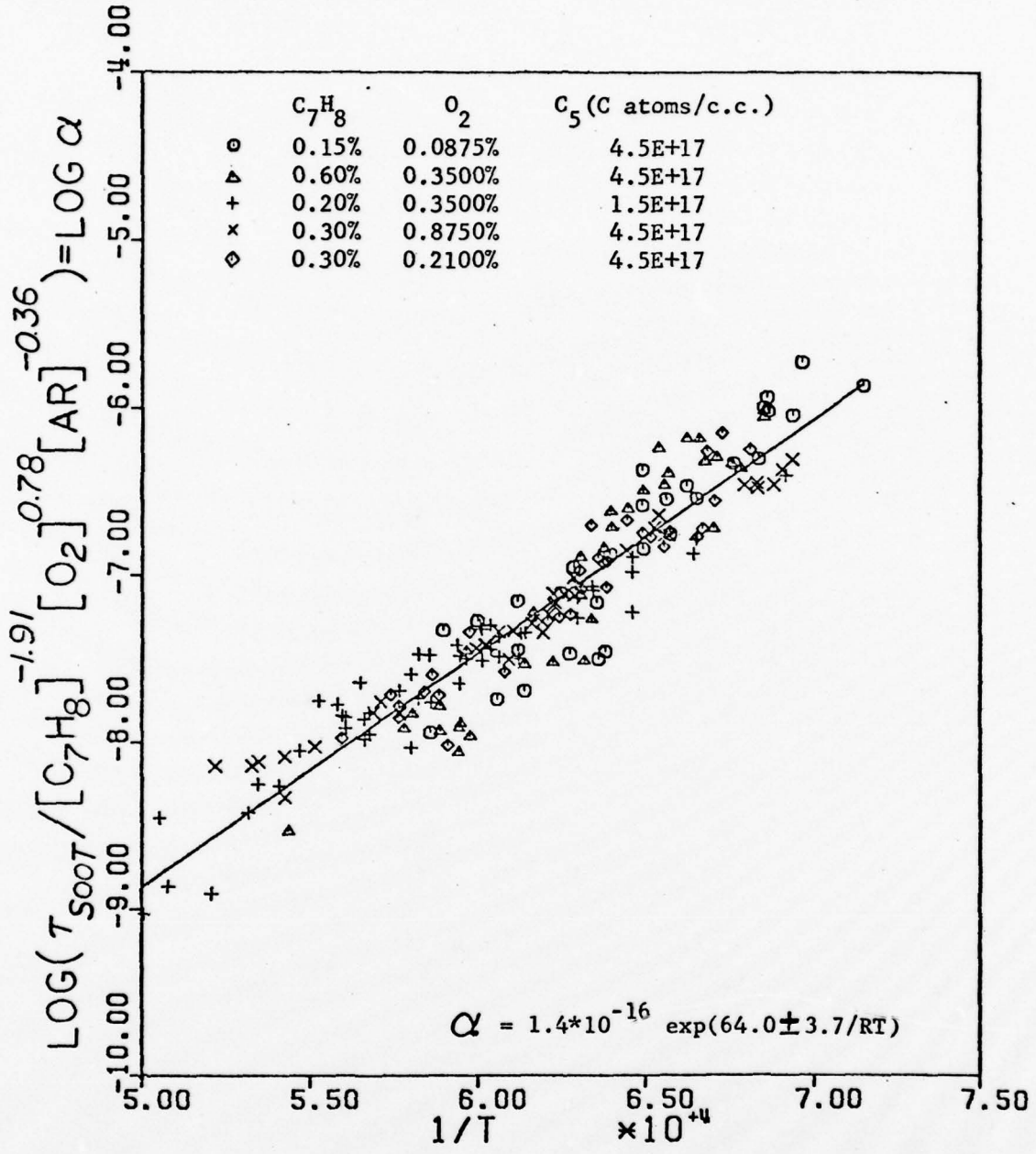

Figure 12. Correlation equation of soot formation delay time study for toluene/oxygen/argon mixtures.

oxygen. The value of -0.36 for c shows that when total pressure increases, the soot forms earlier. This observation is in agreement with the soot yield study; the soot yield increases as the total pressure increases while the temperature is below 1700°K.

Figure 13 shows the soot yield as a function of time for the toluene and toluene/acetylene mixtures. These data indicate that not only more soot is formed from the aromatic, but that it forms faster. This does not preclude some soot forming from the acetylene, but it most certainly is of secondary importance.

Figure 14 shows the same effect of adding oxygen to the toluene and toluene/acetylene systems. The relative values of the rates remain as they were for pyrolyzed mixtures.

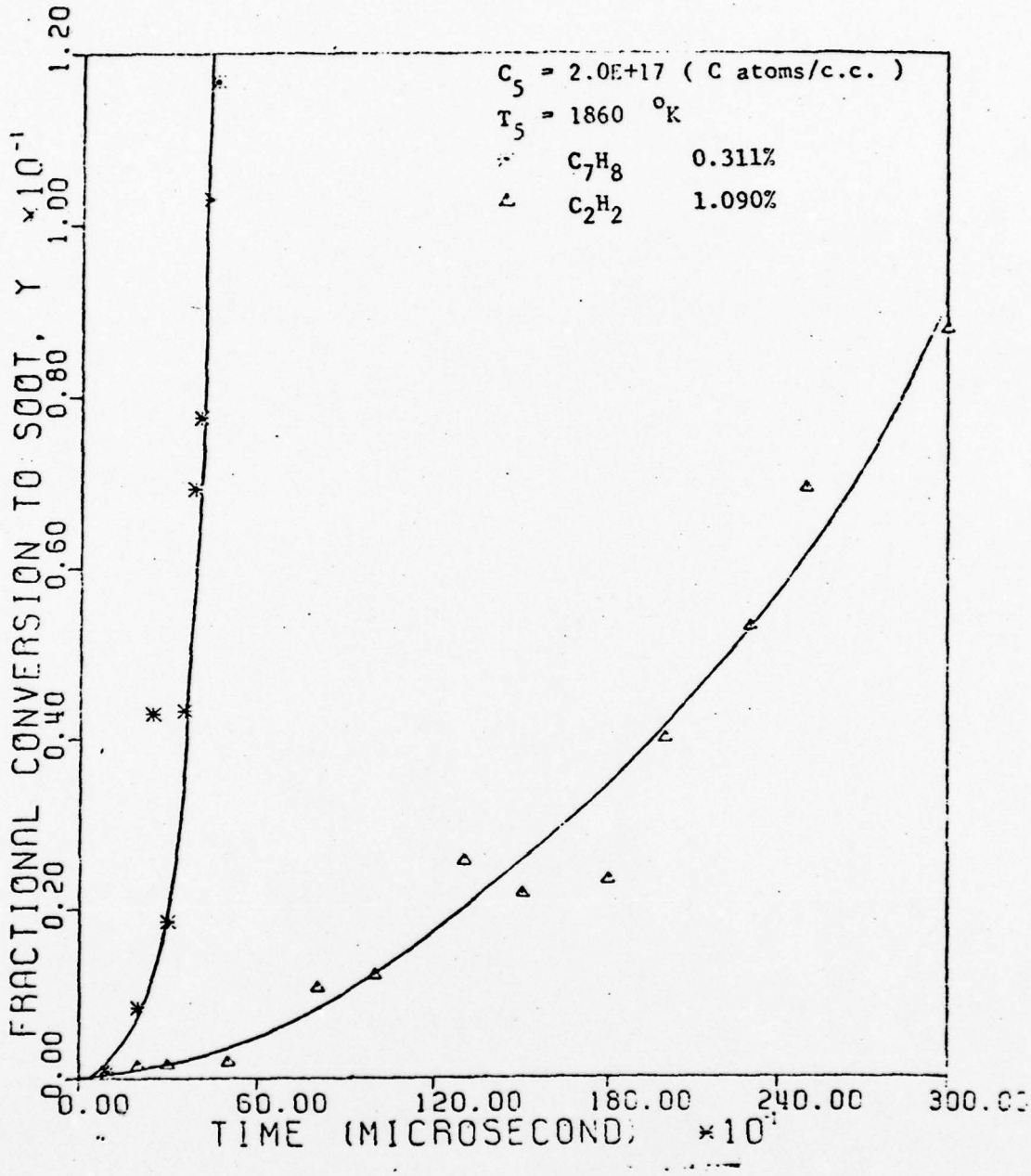

Figure 13. Comparison of soot yields during pyrolysis of acetylene and toluene as a function of time.

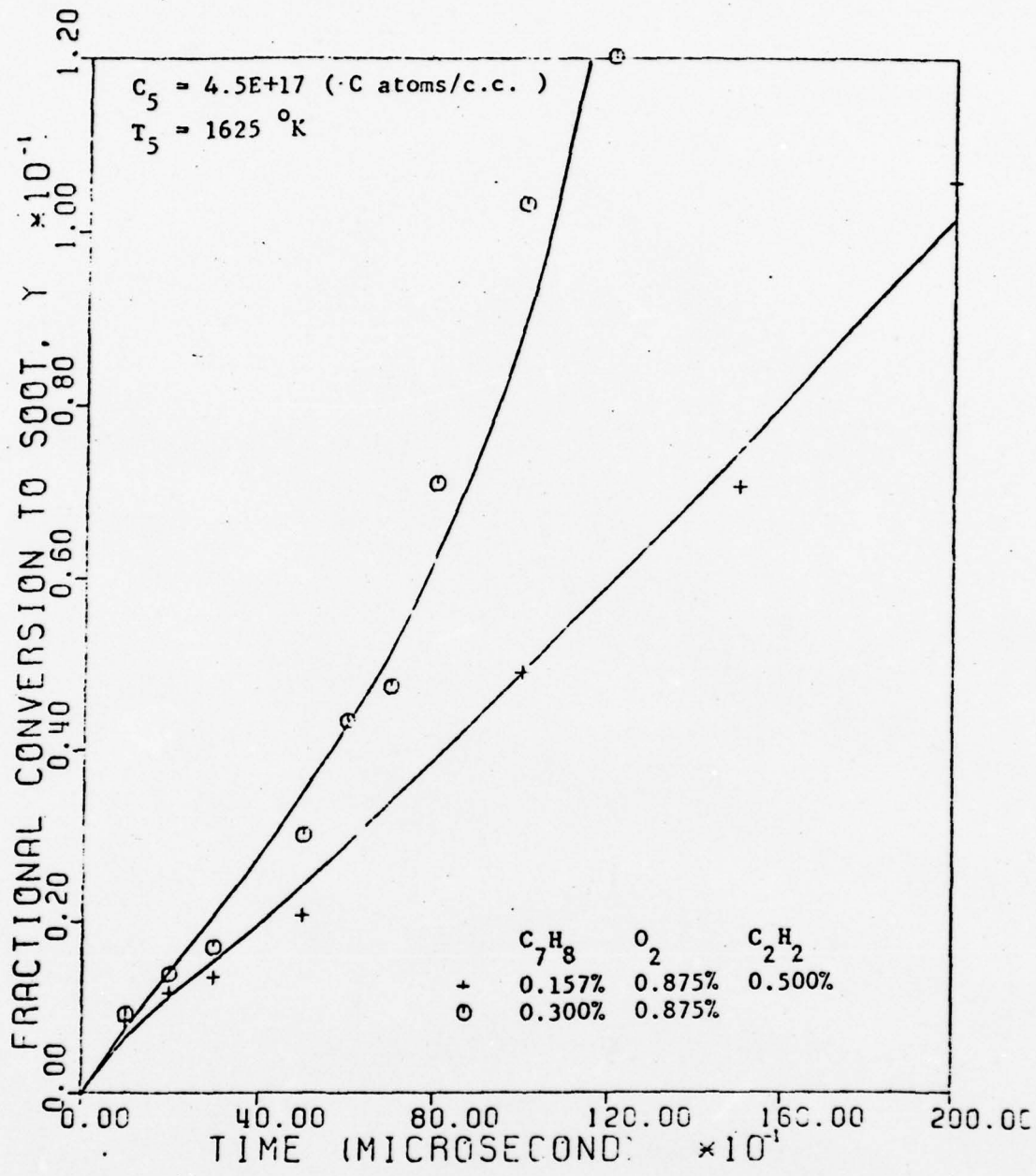

Figure 14. Comparison of soot yields during oxidation of toluene/acetylene/argon mixtures as a function of time.

THERMOCHEMICAL AND KINETIC PROPERTIES OF POLYCYCLIC AROMATIC HYDROCARBONS

The group additivity techniques can be applied to the prediction of standard gas-phase heat of formation, intrinsic entropies, and heat capacities for polycyclic aromatic hydrocarbons (PCAHs) consisting of six-membered rings (28,29). It uses four groups for unsubstituted PCAHs. First one is the C-H group in benzene, $[C_B\text{-}(H)]$; three other groups associated with carbon atoms located at the border of two or three fused rings, C_{BF}, are distinguished, these groups are $[C_{BF} - (C_B)_2 (C_{BF})]$, $[C_{BF} - (C_B)\ (C_{BF})_2]$, and $[C_{BF} - (C_{BF} - (C_{BF})_3]$; e.g. benzopyrene

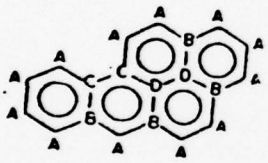

$A = [C_B - (H)]$

$B = [C_{BF} - (C_B)_2(C_{BF})]$

$C = [C_{BF} - (C_B)(C_{BF})_2]$

$D = [C_{BF} - (C_{BF})_3]$

Therefore the thermochemical properties of benzopyrene will be the summation of the thermochemical properties of $12[C_B - (H)$, $4[C_{BF} - (C_B)_2(C_{BF})]$, $2[C_{BF} - (C_B) - (C_B)(C_{BF})_2]$ and $2[C_{BF} - (C_{BF})_3]$ groups. The lack of convergence to graphite for large PCAHs is a possible defect of this scheme. However, it may be smoothed and adjusted by the following method.

The differences of thermochemical properties of PCAHs may be in proportion to the difference of the heat of formation at 297°K (30) e.g.

	Benzene C_6H_6	Naphthalene $C_{10}H_8$	Phenanthrene $C_{14}H_{10}$
$\Delta H_{f,298}$	19.82	35.99	49.46

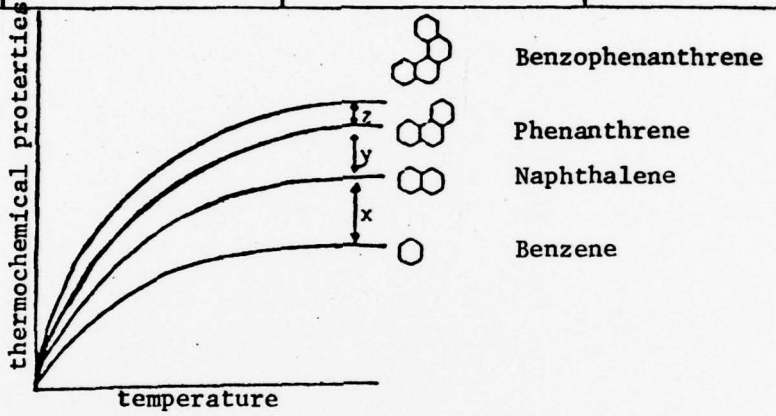

$$\frac{x}{y} = \frac{\Delta H_f,\ C_{10}H_8 - \Delta H_f,\ C_6H_6}{\Delta H_f,\ C_{14}H_{10} - \Delta H_f,\ C_{10}H_8} = \frac{35.99 - 19.82}{49.46 - 35.99} = \frac{16.17}{13.47} \qquad \text{(Eq. 24)}$$

$Z = y + (y-x) = 13.47 - 2.7 = 10.77$

Therefore the thermochemical properties of benzophenanthrene can be estimated by adding an amount of Z to the thermochemical properties of phenanthrene. Constant pressure heat capacity, enthalpy, and entropy are relate to heat of formation data by (Eq. 24).

The heat of formation of PCAH's may be either calculated by Sanderson's Method (31), the group additivity technique, or obtained from experimental data.

Aromatic pyrolysis and combustion may be analyzed by two approaches: 1) empirical correlations and comparisons are established to expedite the direct use of experimental data and the formation of global-rate

equations and 2) detailed mechanistic models for aromatic combustion may be developed. Since the fuel molecules of interest are large, their reactions are very complex and they produce many intermediate compounds and radicals. Toluene is still the typical aromatic fuel for which a detailed kinetics model will be developed.

Pyrolysis and oxidation of many small hydrocarbon molecules have been extensively studied. However, most commercial fuels, either petroleum based or synthetic, are composed mostly of large molecules. Mechanistic kinetic models are not yet available for such large molecules, so global, empirical models are usually used to represent pyrolysis and the early stages of oxidation. These global models are obtained directly from experiments. For aromatic fuels, the key feature in initiating the reactions is the opening of the rings in the structure. The kinetics of several typical fuels have recently been studied in our laboratory. The ignition delay data presented in Figure 15 indicates that toluene is the most difficult to ignite of all of these fuels. All of the data shown are from our experiments (1), so that experimental variations between laboratories will be minimized. Benzene is slightly easier to ignite. Assuming that the initiation reactions for benzene and toluene oxidation are given by

$$C_6H_6 + M \rightarrow C_6H_5 + H + M \qquad \Delta H_r = +105 \text{ kcal} \tag{5}$$

$$\phi CH_3 + M \rightarrow \phi CH_2 + H + M \qquad \Delta H_r = +85.2 \text{ kcal} \tag{6}$$

where ϕ represents the phenyl radical, these experimental results are rather surprising since the benzene initiation is more endothermic than

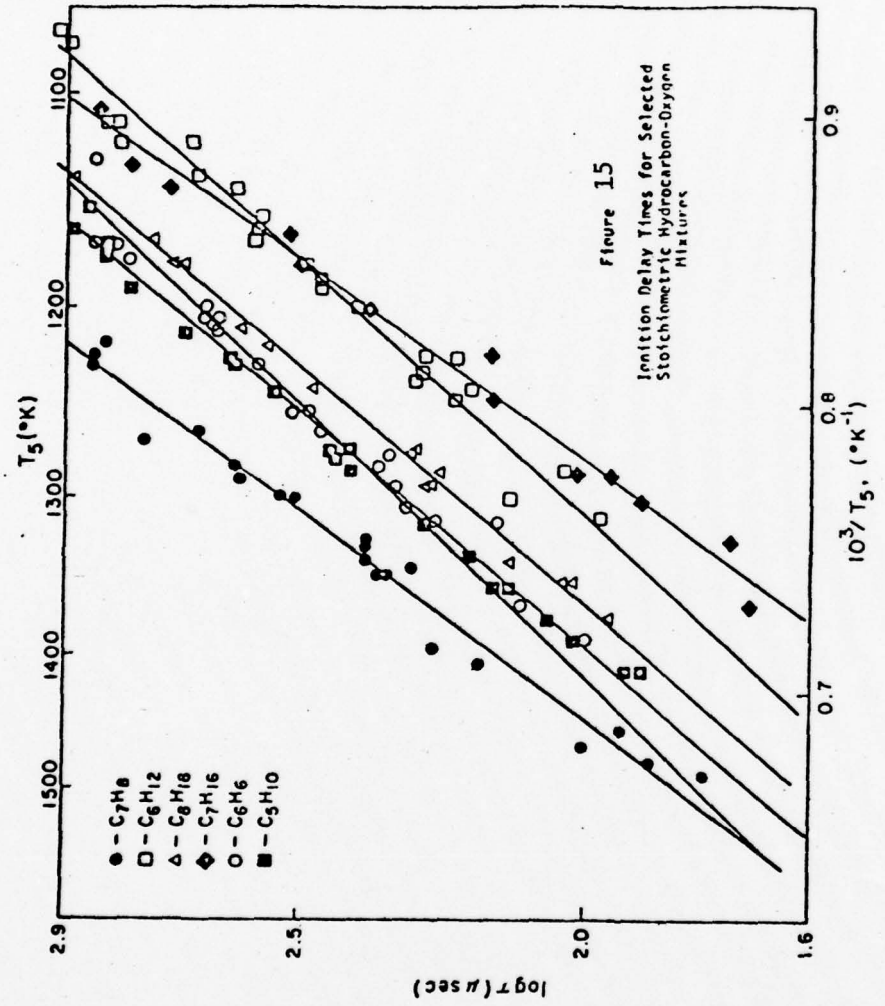
Figure 15
Ignition Delay Times for Selected Stoichiometric Hydrocarbon-Oxygen Mixtures
● - C_7H_8
□ - C_6H_{12}
△ - C_8H_{18}
◆ - C_7H_{16}
○ - C_6H_6
■ - C_5H_{10}
T_5 (°K)
1100
1200
1300
1400
1500
$10^3/T_5$, (°K^{-1})
0.9
0.8
0.7
log τ (μ sec)
2.9
2.5
2.0
1.6

the toluene initiation by approximately 20 kcal. Unimolecular decompositions should not be important in the pressure ranges of most combustion processes. However, if the rate determing oxidation reactions are given by

$$C_6H_6 + OH \rightarrow {}^{H}\!\diagdown\!\phi\!\diagup\!{}^{OH} \rightarrow C_6H_5OH + H \quad \Delta H = -14 \quad \text{kcal} \qquad (7)$$

$$\phi CH_3 + OH \rightarrow {}^{CH_3}\!\diagdown\!\phi\!\diagup\!{}^{OH} \rightarrow C_6H_5OH + CH_3 \quad \Delta H = -17.3 \text{ kcal} \qquad (8)$$

it is easier to understand why benzene has a slightly shorter ignition delay time than toluene. These reactions avoid the route of using HO_2 which we believe is not important at high temperatures. Low temperature kinetics studies are discussed in (2) and (32). The apparent activation energies indicated in Figure 15 are comparable to values previously reported in the literature.

Iso-octane, cyclopentane, and cyclohexane are shown to ignite at very similar rates. If there are any differences in these compounds, the iso-octane is slightly harder to ignite. As expected n-heptane is the easiest fuel to ignite, because its long straight chain is more susceptible to attack by pre-ignition reactions. These measured ignition behaviors are consistant with the usage of aromatics as an octane improver to replace tetraethyl lead in motor fuels.

Golden (33) in a recent report reviews the available information on aromatic oxidation. His suggested scheme for toluene oxidation is

$$\phi - CH_3 + O_2 \rightarrow \phi - CH_2\cdot + HO_2\cdot \qquad (9)$$

$$HO_2\cdot + M \rightarrow H + O_2 + M \qquad (10)$$

$$\phi - CH_3 + O \rightarrow \phi - CH_2 + OH \qquad (11)$$

and the possible decomposition of toluene before oxidation

$$Ar + \phi - CH_3 \rightarrow \phi \cdot + CH_3^{\cdot} + Ar \qquad (12)$$

is excluded because it is too endothermic. However, the large positive argon dependency suggests, but certainly does not prove, that this three-body reaction may be important.

The following preliminary scheme is proposed to describe both oxidation and soot formation under oxidative conditions. First the decomposition reaction already mentioned

$$\phi CH_3 + M \rightarrow \phi CH_2^{\cdot} + H + M \qquad \Delta H = +85.2 \qquad (13)$$

$$\phi CH_3 + M \rightarrow \phi\cdot + CH_3^{\cdot} + M \qquad \Delta H = +100.8 \qquad (14)$$

the radical exchange reactions

$$H + \phi CH_3 \rightarrow H_2 + \phi CH_2^{\cdot} \qquad \Delta H = -19.0 \qquad (15)$$

$$H + \phi CH_3 \rightarrow C_6H_6 + CH_3^{\cdot} \qquad \Delta H = -9.4 \qquad (16)$$

$$CH_3^{\cdot} + \phi CH_3 \rightarrow CH_4 + \phi CH_2^{\cdot} \qquad \Delta H = -19.6 \qquad (17)$$

$$\phi\cdot + \phi CH_3 \rightarrow \phi\text{-}\phi + CH_3^{\cdot} \qquad \Delta H = -12.2 \qquad (18)$$

$$\phi\cdot + \phi CH_3 \rightarrow C_6H_6 + \phi CH_2^{\cdot} \qquad \Delta H = -23.6 \qquad (19)$$

the oxidation branching reactions which start with the following

$$H + O_2 \rightarrow OH + O \qquad \Delta H = +16.9 \qquad (20)$$

$$CH_3^{\cdot} + O_2 \rightarrow CH_3O + O \qquad \Delta H = +28.3 \qquad (21)$$

on the basis that oxygen molecules can be encountered by any radical more than any other species. Finally, toluene oxidation reactions:

$$OH + \phi CH_3 \rightarrow \phi OH + CH_3^{\cdot} \qquad \Delta H = -17.3 \qquad (22)$$

$$O + \phi CH_3 \rightarrow \phi CH_2^{\cdot} + OH \qquad \Delta H = -17.1 \qquad (23)$$

$$OH + \phi CH_3 \rightarrow \phi CH_2^{\cdot} + H_2O \qquad \Delta H = -34.1 \qquad (24)$$

$$\phi\cdot + O_2 \rightarrow (C_6H_5OO^{+}) \rightarrow 2CO + C_2H_2 + C_2H_3 \qquad \Delta H = -11.2 \qquad (25)$$

This last equation was taken with reservations from Asaba's scheme (4) for benzene oxidation. Also note that the scheme predicts the formation of phenol as an intermediate - which is a difficult point to prove.

$$\phi OH + H \rightarrow \phi\cdot + H_2O \qquad \Delta H = -0.6 \qquad (26)$$

$$\phi\cdot + OH \quad H_2O + C_6H_4(\text{benzyne}) \qquad \Delta H = -133.5 \qquad (27)$$

$$C_6H_4 + OH \rightarrow H_2O + C_6H_3 \text{ chain} \qquad \Delta H = -63.6 \qquad (28)$$

$$C_6H_4 + O \rightarrow OH + C_6H_3 \qquad \Delta H = -46.6 \qquad (29)$$

An alternative way to open the ring, rather than the non-elementary step 13 suggested by Asaba is

$$\phi\cdot + OH \rightarrow C_6H_6 + O \qquad \Delta H = -8.53 \qquad (30)$$

$$C_6H_6 + OH \rightarrow \phi\cdot + H_2O \qquad \Delta H = -14 \qquad (31)$$

The oxidation of the other radicals and species

$$C_2H_3 + M \rightarrow C_2H_2 + H + M \qquad \Delta H = +40.4 \qquad (32)$$

$$C_2H_3 + OH \rightarrow C_2H_2 + H_2O \qquad \Delta H = -78.9 \qquad (33)$$

$$C_2H_3 + O \rightarrow C_2H_2 + OH \qquad \Delta H = -61.9 \qquad (34)$$

$$CH_3O + M \rightarrow CH_2O + H + M \qquad \Delta H = \text{not available} \qquad (35)$$

$$CH_3O + O \rightarrow CH_2O = OH \qquad \Delta H = -79.2 \qquad (36)$$

$CH_2O + M \rightarrow CHO + H + M$ $\Delta H = -0.5$ (37)

$CHO + M \rightarrow CO + H + M$ $\Delta H + +16.7$ (38)

and finally ecombination reactions

$2C_6H_5 \rightarrow C_{12}H_{10}$ $\Delta H = -113.5$ (39)

$2\phi CH_2 \rightarrow \phi-CH_2-CH_2-\phi$ $\Delta H = -55.6$ (40)

$M + C_6H_3 + H \rightarrow C_6H_4(chain) + M$ $\Delta H =$ not available (41)

$M + C_6H_3 + CH_3 \rightarrow C_7H_6(chain) + M$ $\Delta H =$ not available (42)

The CO/CO_2 ratio formed during oxidation of aromatics is believed to be important and measurable. This is in agreement with (32).

More thermodynamic and kinetic data need to be collected and estimated for the reactions, radicals, and stable species of interest.

CLOSURE

Aromatic-fuel ignition-delay comparisons, a correlation equation for toluene ignition delays, soot formation conditions, soot formation delay times, and a preliminary analysis of combustion mechanisms are presented.

The correlation equation for ignition-delay times for toluene reported herein differs substantially from one reported by other investigators. We believe our values are correct, but we cannot yet explain the differences in these observations. Two important factors in ignition-delay measurements from shock-tube experiments are the location of the combustion detector devise and the conversion of lapse-time data into test gas temperature. Both of these factors were careful consideration in our experiments. Further analysis of the experiment is continuing to determine the accuracy of ignition-delay time measurements in shock-tube experiments.

Soot-formation delay-time data are presented and are believed to be accurate. The amount of soot formed is deduced from a calculation; these results are known to predict more soot than is actually present. No evidence was found to indicate that the aromatic ring had to be broken before soot could be formed.

An IR spectral window was found which can be used to monitor the decrease of toluene molecules in a mixture. This effect has not been proved to be quantitative by a collaborating experiment. Specifically, it remains to be verified that this observation is a concentration effect and not a temperature effect on the absorption coeffect of the gas.

WRITTEN PUBLICATIONS

The following manuscript has been accepted for publication in Combustion and Flame. "Comparative Ignition Delay Times for Selected Ring-Structured Hydrocarbons", A. Burcat, R. C. Farmer, R. L. Espinoza and R. A. Matula.

The following manuscripts are being prepared for publication.

1. "Kinetics of the Ignition Delay Time of Toluene in a Shock Tube", A. Burcat, R. C. Farmer and R. A. Matula. For submission to Combustion and Flame.
2. "Incipient Soot Formation during Oxidation", T. S. Wang, R. C. Farmer, and R. A. Matula. For submission to Journal of American Chemical Society.

PROFESSIONAL PERSONNEL

Principal Investigators:

Professor R. A. Matula

Professor R. C. Farmer

Graduate Students:

Ten-See Wang, Ph.D. Candidate

Rafael Espinoza, Ph.D. Candidate

Viro Vilimpochapornkul, M.S. Candidate

INTERACTIONS

Continuous contact with the Thermodynamic Research Center (TRC) at Texas A&M University is maintained. TRC is maintaining thermodynamic data for the American Petroleum Institute. Our contact with this agency and our advising them of the temperature range for which we need property data has resulted in a joint effort whereby their property calculations are now extended to the higher temperature ranges needed for combustion analysis.

Contact is also maintained with Drs. W.S. Blazowski, Exxon; R.B. Edelman, SAI; H.F. Calcote, AeroChem; and Don Kern, UNO, all of whom are conducting investigations of direct bearing on aromatic pyrolysis and combustion.

APPENDIX A

TEST FACILITIES

The Experimental Facilities in the combustion laboratory of Louisiana State University include two shock tubes with associated electronic, optical, and gas chromotographic equipment.

Conventional Shock-Tube Facility

The conventional shock-tube experiments are conducted in a 7.6 cm diameter stainless steel shock-tube, which is schematically shown in Figures A-1 and A-2. The shock tube is fitted with a double diaphragm system. The driven section of the tube is 7.3 m long and the driver section is 3 m in length. The tube is fitted with an Edwards "Speedivac" E04 oil diffusion vacuum pump system which allows the tube and associated gas manifold to be evacuated to 2E-05 torr (measured near the end cap of the driven section of the shock tube). The incident shock velocity is measured, in a standard manner using the voltage signal generated by Atlantic Research LD-25 pressure pulse transducers to trigger a digital storage timer. The arrangement of these transducers is shown in Figure A-3. Transit times between transducer stations were measured to within 1 microsecond (μsec).

The digital storage timer used to measure the incident shock velocity was driven by a 10MHZ crystal oscillator. The first trigger station starts the counter and the operation of subsequent stations causes the value of the count to be written onto digital memory with a storage delay of less than 300 ns. This results in a net uncertainty of 1 μs for all the time intervals. Trigger signals from pressure transducers which produce voltage proportional to the pressure jump due to shock wave

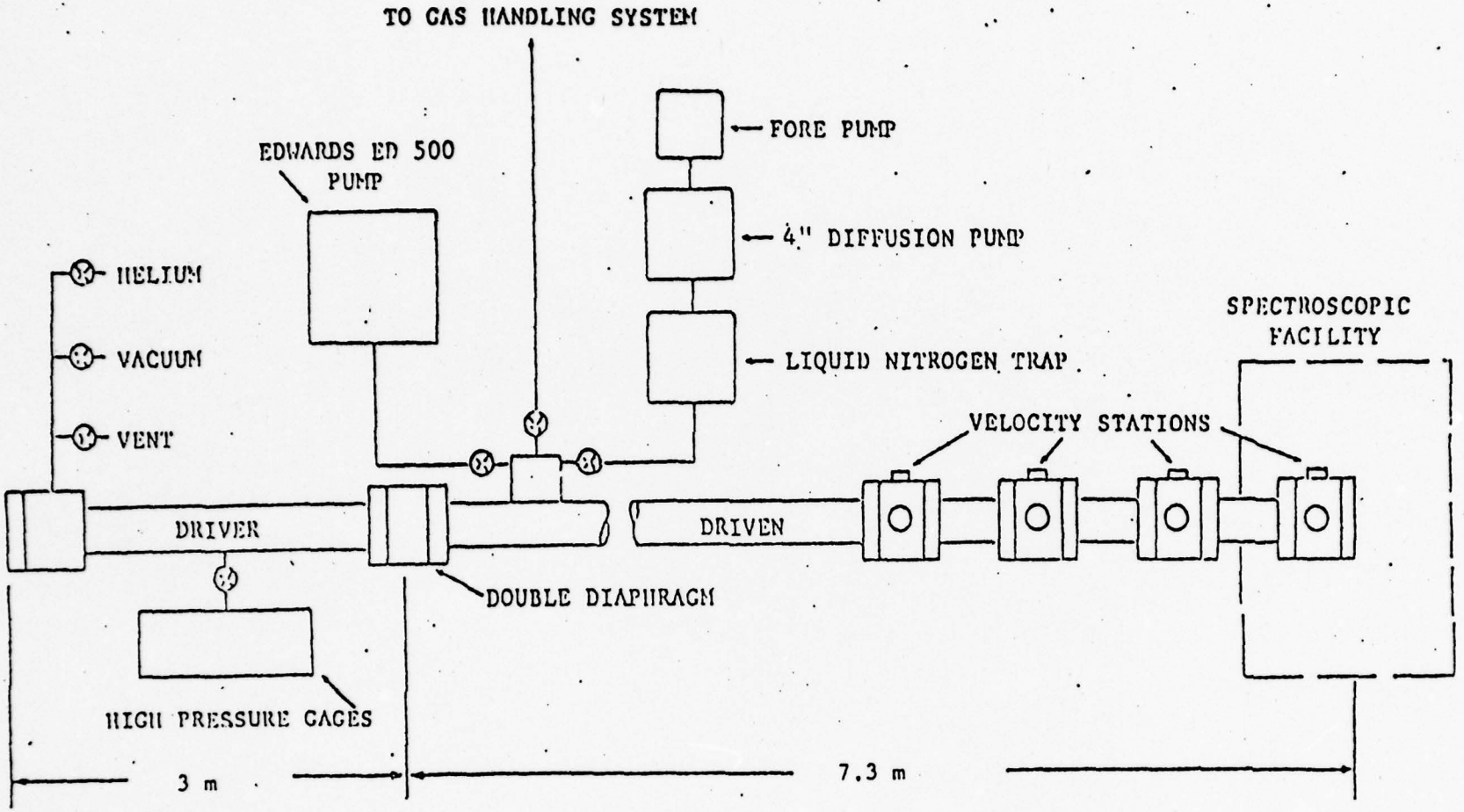

Figure A-1 -A Schematic of the Conventional Shock Tube Facility

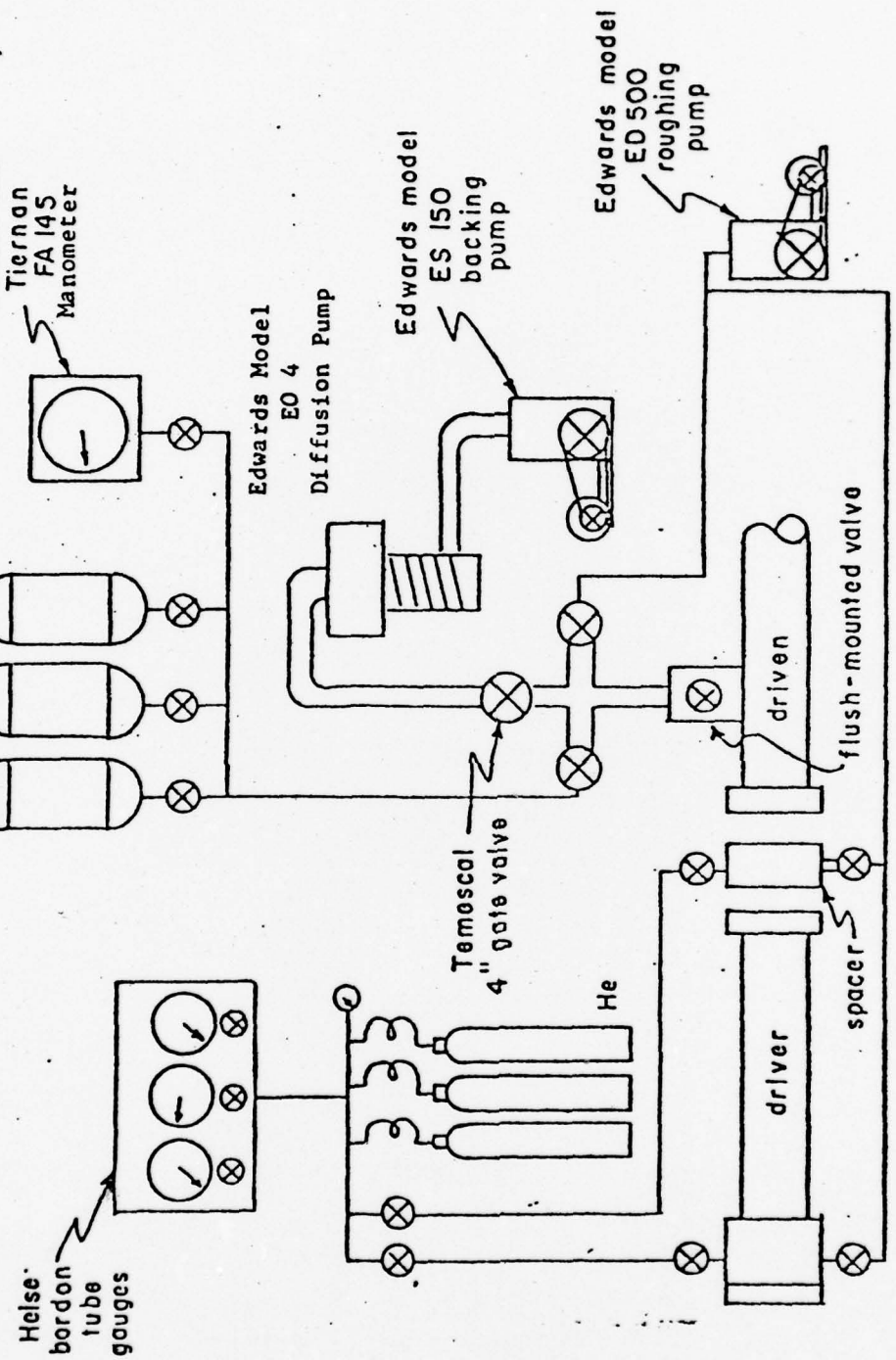

FIGURE A-2 SCHEMATIC OF SHOCK TUBE GAS HANDLING AND VACUUM SYSTEMS

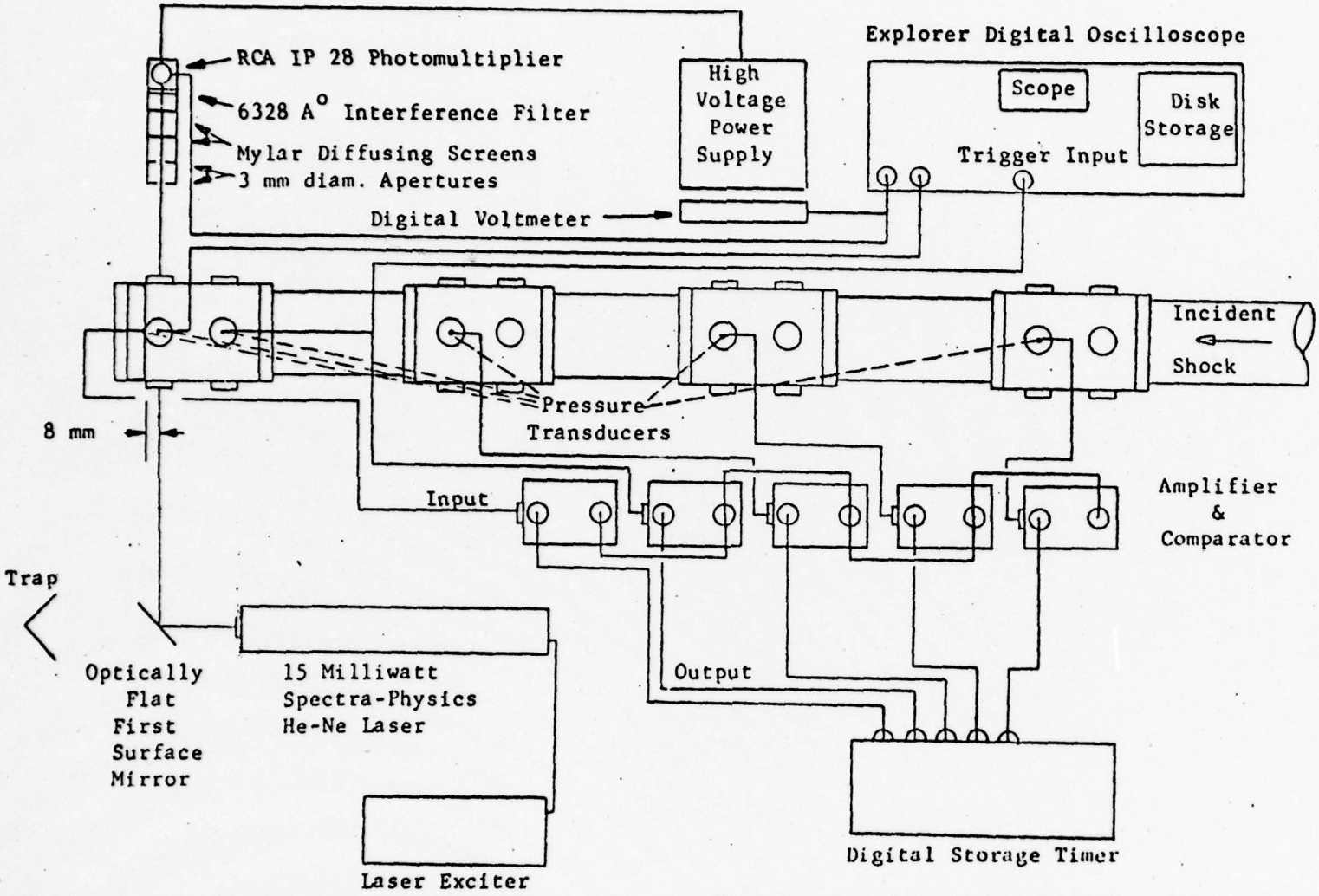

Figure A-3 Schmatic of Experimental Apparatus for the Measurement of Incipient Soot Formation

passage are preprocessed through an amplifier and comparator circuit to be compatible with the internal transitor-transitor-logic (TTL) operation of the counter.

An adjustable end plug was made such that the end wall can be placed as close to the spectroscopic abservation station as possible e.g. the first plug was designed so that the axis of optical measurements passed diametrically across the shock-tube at a position about 9 mm in front of the end wall. A second plug which places this path along the end wall is now available.

Single-Pulse Shock Tube Facility

The 2.54 cm diameter single-pulse or chemical shock tube, shown in Figure A-4, is utilized to determine quenched product and reactant distributions and ignition delay times. The driver section of the tube was constructed of stainless steel. The length of the driver is adjustable from 0.30 m to 1.52 m in increments of 5 cm by the insertion of appropriate plugs. A 4 m driven section constructed primarily of pyrex conical piping with three stainless steel stations located in the final 0.70 m. The driven section contains piezoelectric transducers, a sampling port, and a ball valve which served to isolate a test sample in the end of the shock tube. A single diaphragm is used to separate the driver and driven sections of the shock tube.

The shock tube is fitted with an Edwards "Speedivac" E02 oil diffusion pump system that is capable of evacuating the driven section to less than 5E-05 torr, measured at the inlet to the diffusion pump. As in the conventional shock tube, incident shock velocity was measured with pressure transducers which were used to trigger interval timers to within a resolution of 1 μsec. Experimental dwell times and quenching rates are determined by analyzing an oscillograph record

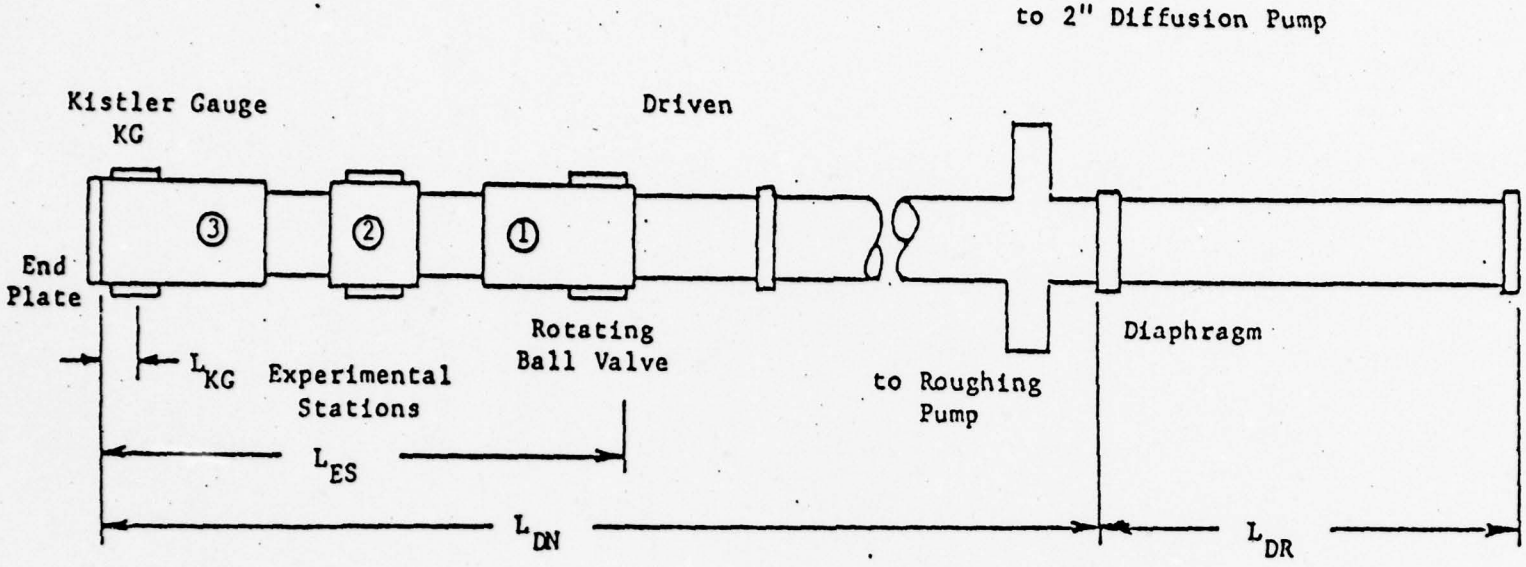

L_{DN} = 406 cm L_{DR} = 30-152 cm

L_{ES} = 70 cm L_{KG} = 5.2 cm

Figure A-4 A Schematic of the Single-Pulse Shock Tube Facility

of the voltage signal from a Kistler type 603A Piezolectric pressure transducer located either on or approximately 5 cm from the end wall of the shock tube, see Figure A-5. The pressure signal was displayed on a Lavoie model 265A oscilloscope fitted with a 265L vertical amplifier.

After quenching, the partially consumed reactants and reaction products are drawn into an evacuated 100 cc glass bulb for subsequent analysis.

Optical Systems

Three types of optical systems are available for in situ measurement; these are a spectral radiometer, filter-detector combinations, and a laser absorption system. Two emission and one absorption measurement can be made simultaneously on the conventional shock-tube.

The major piece of optical equipment is a modified spectral radiometer donated by NASA. The essential features of the spectral radiometer is the Perkin Elmer model 99 Prism Monochromator and the built-in blackbody calibration source. (Figure A-6 and A-7). The blackbody source facilitates in the quick change-over operation, when switching between U.V. and I.R. regions, which consists of simple realignment of the monochromator's mirror. The prism is a Lithium Fluoride crystal with a useful range of from approximate 300 nm to 6 μ. This monochromator is interchangable with a Perkin Elmer model 98G Grating Monochromator which we use. While the Prism Monochromator is an extremely useful tool for spectral scan to select the most promising wavelength to be used in the gathering of kinetic data, the Grating Monochromator can be used to increase signal strength and obtain better dispersion once a suitable wavelength has been

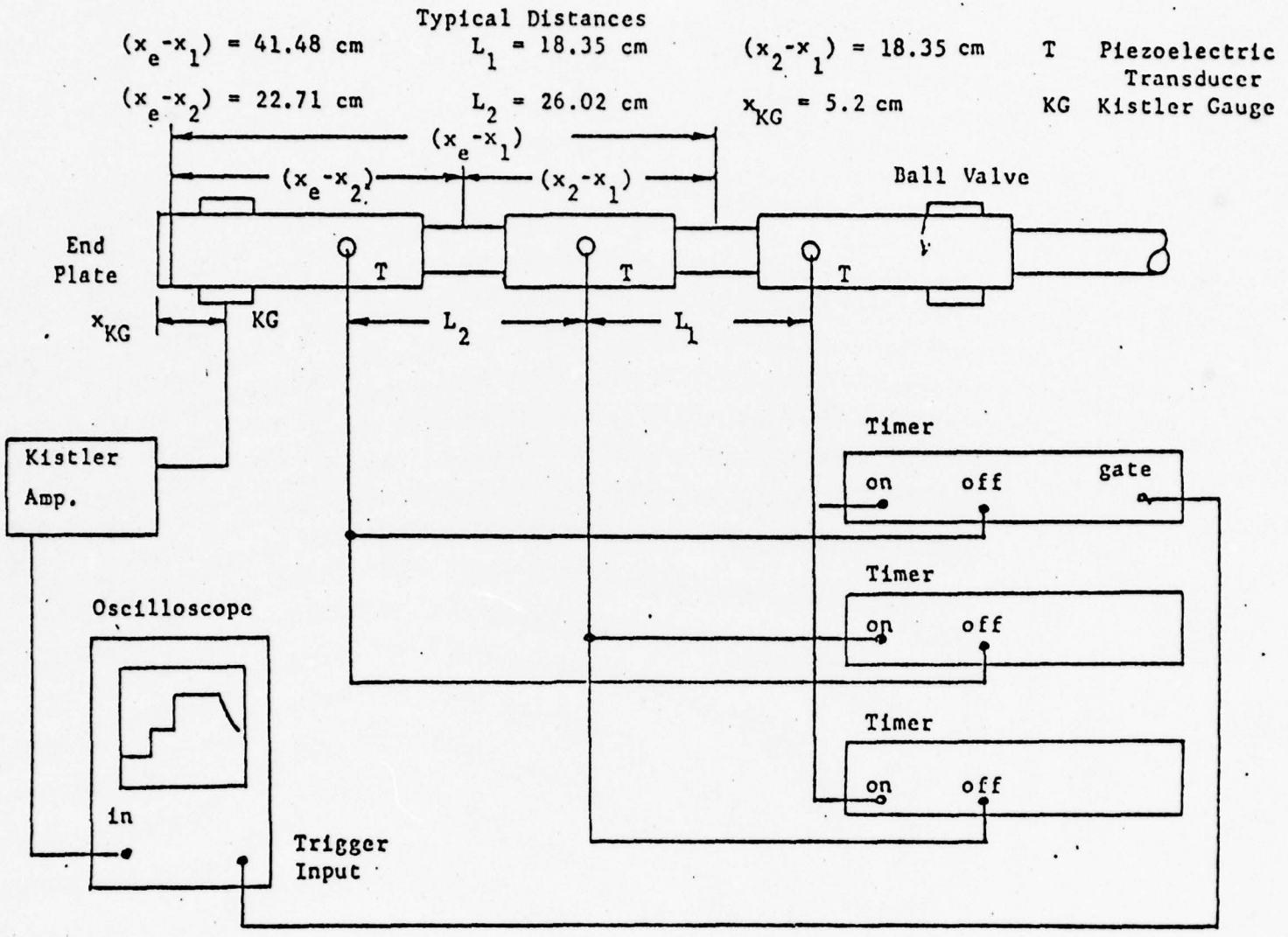

Figure A-5- A Schematic of the SPST Instrumentation

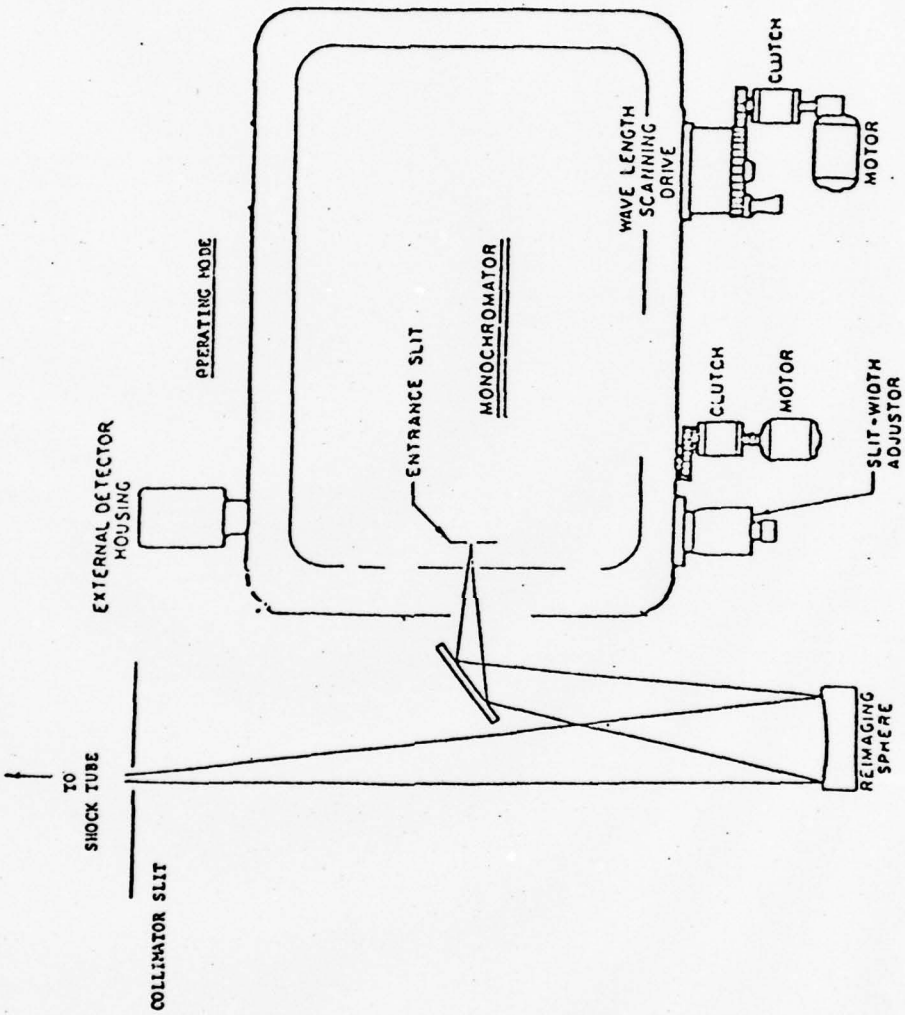

Figure A-6 - Schematic Diagram of Spectral Radiometer

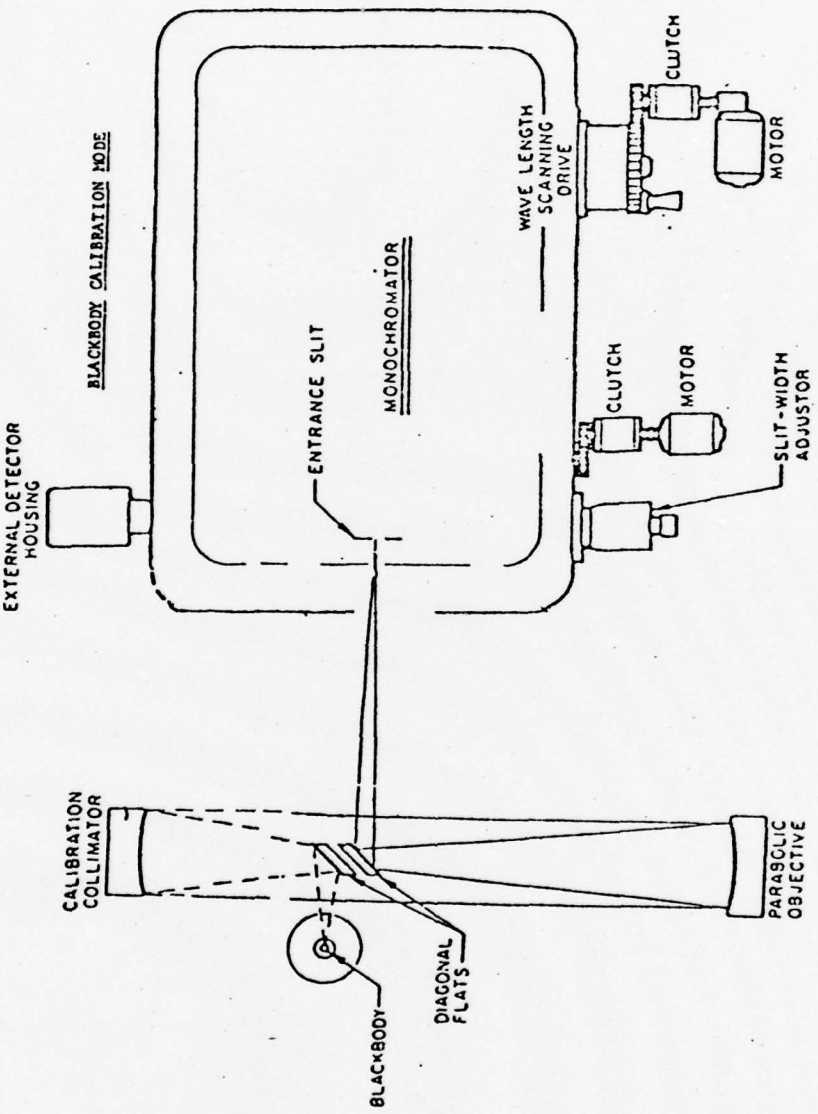

Figure A-7 - Schematic Diagram of Spectral Radiometer

located. The grating is blazed at 3.75 μ; the price of another grating is comparable to that of an interference filter. This is a major advantage since it allows us to increase the resolution and vary the wavelength at a modest cost.

For operation in the I.R. region the spectral radiometer's output radiation is focused by a concave 90° focusing mirror onto a side looking Texas Instrument Indium Antimonide (InSb) detector with a useful range of from 1.0 to 5.5 um. A Perry model 720 Amplifier processes the signal from the detector and amplified it 100 times. The signals are displayed and recorded digitally on a Nicholet Explorer II Digital Oscilloscope.

This oscilloscope has 2 data channels with total recording space per channel of about 2000 data points. The data are stored on floppy magnetic disckettes with 8 tracks per disc. Present use of discs has been extremely economical and convenient in data reduction. Price per disc is about $5.00.

Radiation in the U.V. region is followed by an EMI type 9785B Photomultiplier Tube. The photomultiplier's spectral range is from 185 to 830 nm, with a typical rated gain of 5×10^6. Currently, the prism monochromator is unable to utilize the lower range of the photomultiplier; substitution of the prism monochromator with a grating monochromator should remove this limitation.

Besides the spectral radiometer, two Indium Antimonide end looking type detectors are available which can be mounted directly onto an observation port on the shock tube, thus providing the capability to measure 2 wavelengths simultaneously (when used in conjunction with the spectrometer). A Gold-doped Germanium I.R. detector from Santa Barbara Research Center which can be used in the range of 2.0 to 8.0 μ

and Mercury-Cadmium Telluride I.R. detector and matching pre-amplifier from I.R. Associates extends the observation range to about 14.0 μ. Spectral width for these detectors are generally defined by stock interference filters purchased from OCLI. Our stock of filters consists of some narrow and long pass filters at 3.4, 4.8 and 5.05 um.

He-Ne laser

A schematic of the He-Ne laser system is shown in Figure A-3. The obsorption of the beam from a 15 milliwatt continuous wave He-Ne Spectra-Physics laser (centered at 6328Å) is used to detect the presence of soot. The laser beam was located so that the axis of the beam passed diametrically across the shock tube. The laser light was spread across the cathode of a IP28 photomultiplier by two mylar diffusers about 3 cm apart. Two 3 mm diameter apertures about 2 cm apart was placed at the front part of the detector housing to ensure that the light striking the photomultiplier originated from the shock tube and not stray sources. A 100(Å) half-width interference filter centered on the laser wavelength defined the optical bandpass so that continuum emission from the glowing shock gas did not contribute to the signal.

Since young soot particles are reported (16) to be spherical in shape and usually less than 300(Å), in diameter, the small particle limit of Mie (26) theory applies; hence, the threshold for soot detection is expected to be independent of temperature. Also, the ratio of scattering efficiency to extinction efficiency is estimated to be very small; so soot is considered to be only an emitter and absorber. The emission signal from soot has been shown to be very small and can be neglected (21).

The measurements were made behind the reflected shock wave in order to obtain a high temperature, isothermal optical path. Maximum test times approximately 4 milliseconds were available during these experiments. The maximum test time was determined by the time between shock arrival and the arrival of the expansion wave at the test station.

Gas Analysis Facilities

The quenched samples are analyzed by gas chromatography. Both flame ionization and thermal conductivity detectors are required to obtain maximum sensitivity for both the hydrocarbons produced by the reactions of interest and the fixed gases. An overview of gas chromatographic techniques is given by Keating (34), and the current gas chromatographic facilities, available are now described.

The product distribution of aromatic pyrolysis of aromatics will be studied with a Perkin Elmer 990 Thermal-Conductivity Gas Chromatograph, and a Perkin Elmer 990 Flame Ionization Detector, gas chromatograph. Five different columns have been used to detect products from the pyrolysis of toluene. In all columns, the carrier flow rate is 30 cc/min.

APPENDIX B

WALL EFFECTS IN CONVENTIONAL SHOCK TUBE FLOW

Temperature, pressure and density are the most important parameters in any chemical kinetics shock tube study. Temperatures in shock tube experiments are rarely measured directly; hence they must be computed by solving the conservation equations of mass, momentum and energy along with the equations of state across a shock wave. The ratios of temperature, pressure and density across a shock front can be solved explicitly in terms of the incident Mach number. Therefore, it is well recognized that an accurate measurement of the incident shock speed in the shock tube is required for accurate determination of the state of the post-shock test gas.

In ideal shock-tube theory, the assumptions of inviscid, steady, one-dimensional flow of an ideal, non-conducting gas with no body forces or boundary layer effects upon the rupture of the diaphragm are made. The shock wave and contact surface start impulsively from rest and travel with constant speeds, U and Uc, respectively. However, in real shock-tube flow, the measured shock speeds are observed to attenuate due to the effect of friction and boundary layer growth along the tube wall (35-37). The incident shock speed at the end wall of the shock tube, where reflection occurs, is less than the average speed at the measurement stations, and the actual temperature and pressure behind the reflected shock wave are less than those computed assuming no attenuation. Previous investigations on the wall effects in shock tube flow were either not convenient to use in converting time of arrival measurements to wave speeds or were based upon a poor assumption, namely, that the distance corresponding

to the measured average speed occurs at the linear average of the distance between two stations (35,38).

A practical attenuation analysis was developed to determine the incident shock speed at the end wall of the tube, computations were based on an empirical shock wave attenuation correlation originally proposed in the form of a pressure ratio exponential decay by Emirch and Wheeler (36):

$$P_{21} - 1 = (P_{21} - 1)_0 \quad \exp(-\bar{C}\, x/D) \tag{B.1}$$

where shock strength P_{21} is the ratio of pressure behind the shock (P_2) to pressure ahead of the shock (P_1). D is the hydraulic diameter of the shock tube, x is the distance measured from the diaphragm and $\bar{C}$ is an experimentally determined constant.

Since the incident shock speed is proportional to the shock strength this correlation was later modified to a more practical form:

$$U_x = U_o \exp(-Ax) \tag{B.2}$$

where U_x is the wave speed at a distance x downstream from the diaphragm, U_o is the initial wavespeed at shock formation on the assumption that the formation processes were completed at the position of the diaphragm, and A is defined as the attenuation factor due to the wall effects.

Suppose there are m time-of-arrival measurement stations in the shock tube the average wavespeed calculated from the data at adjacent measuring stations is

$$\bar{U}_{n,n+1} = \frac{X_{n+1} - X_n}{t_{n+1} - t_n} \tag{B.3}$$

where t_n is the time read from the timer at station n. By definition

$$\bar{U}_{n,n+1} = \frac{1}{X_{n+1} - X_n} \int_{X_n}^{X_{n+1}} U_x dx \tag{B.4}$$

Substitute equation (B.2) to equation (B.4), we have

$$\bar{U}_{n,n+1} = \frac{1}{X_{n+1} - X_n} \int_{X_n}^{X_{n+1}} U_o \exp(-Ax)dx$$

$$= \frac{-U_o/A}{X_{n+1}-X_n} \left[\exp(-AX_{n+1}) - \exp(-AX_n) \right] \qquad \text{(B.5)}$$

Taking the summation of the average wavespeed and divide it by any one average speed, e.g., $\bar{U}_{1,2}$, the following basic equation for the computation of the attenuation factor is obtained, where the left hand side can be calculated from the time of arrival measurements and the right hand side is obtained from equation (B.5).

$$\frac{\sum_{n=1}^{m-1} \bar{U}_{n,n+1}}{\bar{U}_{1,2}} = \frac{\sum_{n=1}^{m-1} \left[\frac{\exp(-AX_{n+1}) - \exp(-AX_n)}{X_{n+1} - X_n} \right]}{\left[\frac{\exp(-AX_2) - \exp(-AX_1)}{X_2 - X_1} \right]} \qquad \text{(B.6)}$$

Let

$$R = \sum_{n=1}^{m-1} \bar{U}_{n,n+1}/\bar{U}_{1,2} \qquad \text{(B.7)}$$

Rearranging equation (B.6), we have

$$A = -\frac{1}{X_2} \text{Alog} \left\{ \left(\frac{X_2 - X_1}{R - 1} \right) \left\{ \sum_{n=2}^{m-1} \left[\frac{\exp(-AX_{n+1}) - \exp(-AX_n)}{X_{n+1} - X_n} \right] \right\} + \exp(-AX_1) \right\} \qquad \text{(B.8)}$$

Let

$$f(A) = A \qquad \text{(B.9)}$$

$$g(A) = \text{Right hand side of equation (B.8)} \qquad \text{(B.10)}$$

The attenuation factor can then be obtained from solving equation (B.9) and (B.10) by an iterative search procedure. The flow diagram of such a search procedure is given in Figure B.1.

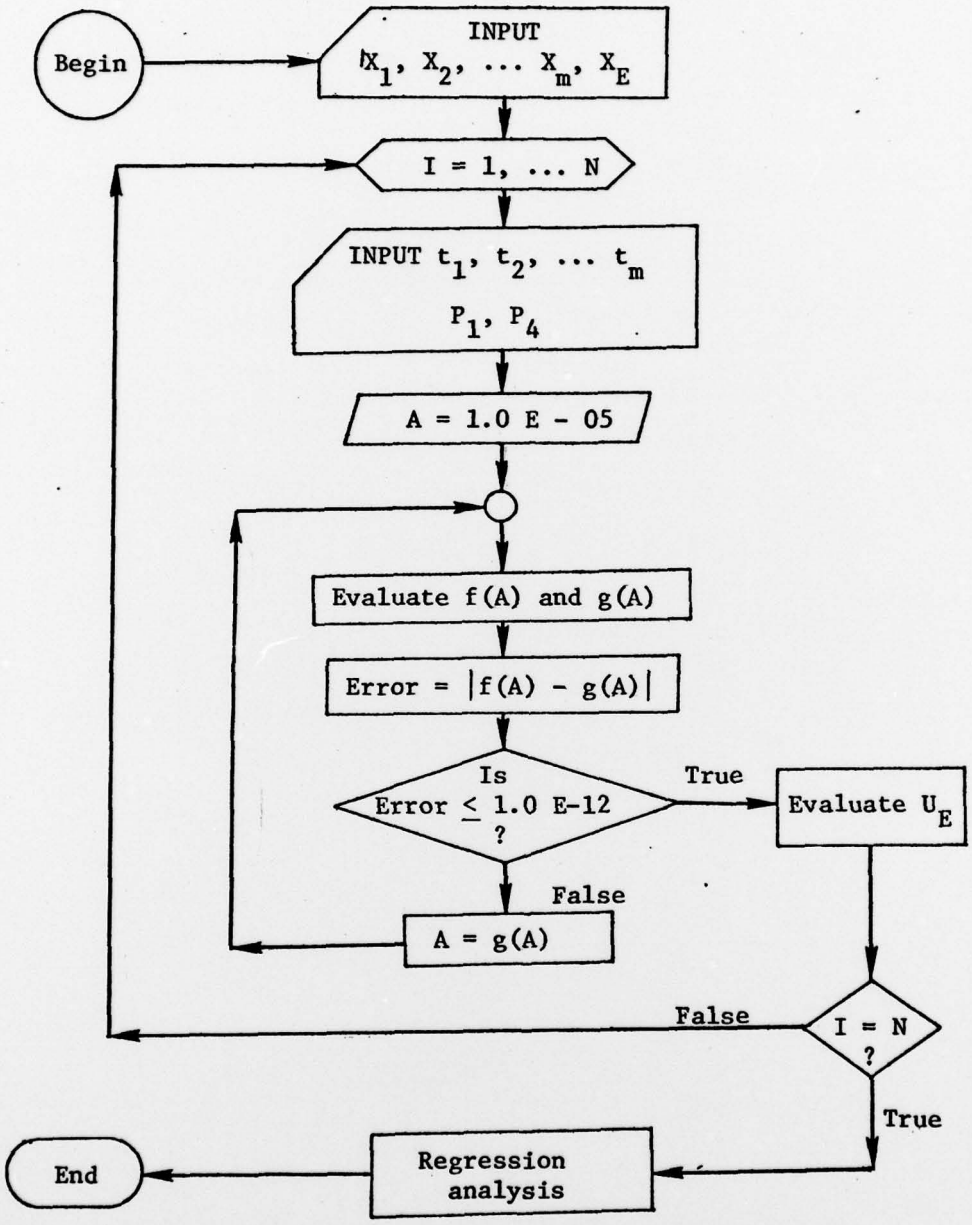

Figure B.1 An iterative search flow diagram for the calculation of shock speed at end wall.

After A is obtained, U_o can be calculated from equation (B.5). The wavespeed of the incident shock at the end wall can then be calculated by substituting X_E into equation (B.2), i.e.,

$$U_E = U_o \exp(-AX_E) \tag{B.11}$$

Where U_E is the distance measured from the diaphragm to the end wall of the shock tube. The distance corresponding to the measured average speed between stations can also be calculated from equation (B.2). It should be emphasized that unlike the other investigations (35,38), the assumption that the distance corresponding to the measured average speed occurs at the linear average of the distance between two stations is not used. Equation (B.6) is used to avoid this poor assumption and yield a more realistic attenuation model.

Figure B.2 shows the experimental attenuation and calculated exponential decay variation of shock speed with distance downstream of diaphragm from a typical shot. Notice that the line plotted in Figure B.2 is not linear. The middle line in each rectangular region corresponds to the average speed measured in each interval. The height of the rectangular regions represents the uncertainty in measured wavespeeds due to the $\pm$ 1 μsec uncertainty from the digital storage timer. The first four data points represent the calculated downstream distance corresponding to the measured average shock speed. The fifth data point is the calculated shock speed at the end wall, which was determined by the average wavespeeds measured for that very shock. The uncertainty range in last interval is bigger than the others since the distance of that interval is smaller than the others.

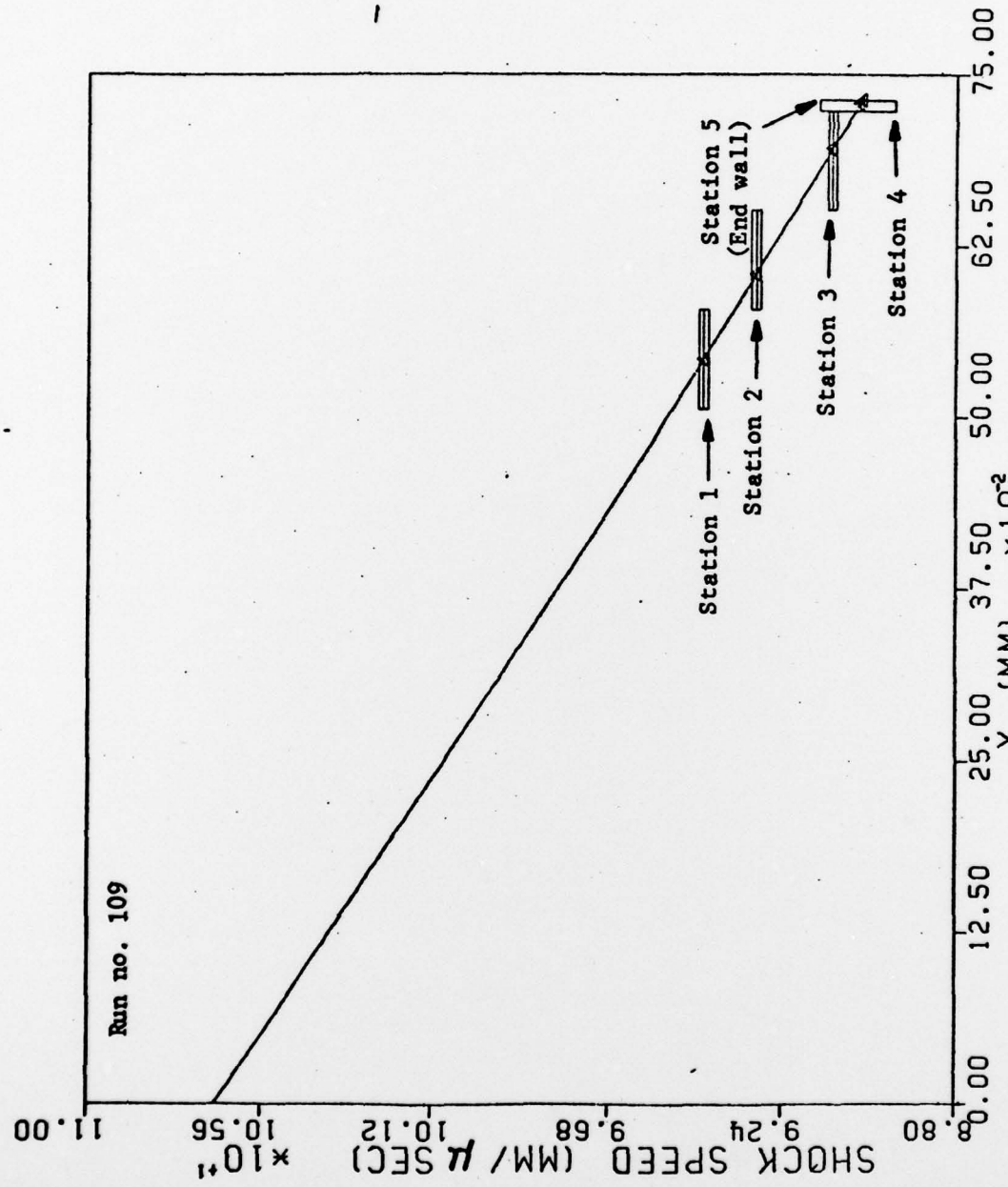

Figure B.2. Experimental and calculated exponential decay variation of shock speed with distance downstream of diaphragm for a typical shock.

The calculated incident shock speed at the end wall was shown to be within the uncertainty range of last measurement interval.

A multivariable, linear regression analysis subroutine (39) is used with the attenuation program to determine the primary relations for U_o, A and U_E as a function of shock strength (P_4/P_1) for different composition mixtures, where P_4 is the initial pressure in the driver section. Notice that the shock strength defined herein is different from the (P_4/P_1) ratio used by Emirch and Wheeler (36). Since (P_4/P_1) can be selected by running a preshock program along with performing a set of preshoot experiments, any desired shock conditions can be achieved. P_4 is the controllable factor in double diaphragm mode operation; hence (P_4/P_1) is viewed as the appropriate representation of the shock strength during the experiment. Figure B.3 shows both U_o and U_E as a fifth order polynomial function of shock strength for toluene/argon mixture shocks. We can see that the curve bent downward at two extremes of the shock strength region tested e.g., at higher values of P_4/P_1 the diaphragm becomes thicker therefore requiring some measurable energy to break the diaphragm. However, this correlation can be highly useful in selecting experimental test conditions, since the shock strength (P_4/P_1) can be adjusted so that a desired shock speed can be achieved. Figure B.4 shows U_o and U_E as a function of P_2/P_1, it is a linear relationship as expected. The regression fit for U_o was not as good as for U_E in both figures. This is not surprising, since it was extrapolated further from the measurement stations.

Figure B.5 shows there is no significant relationship between the attenuation factor and the shock strength statistically speaking, the expected value of the attenuation factor will be the average of those data points. The primary factors which contribute to the scattering of the data may be due to (1) the inconsistency of the break strength of the diaphragm

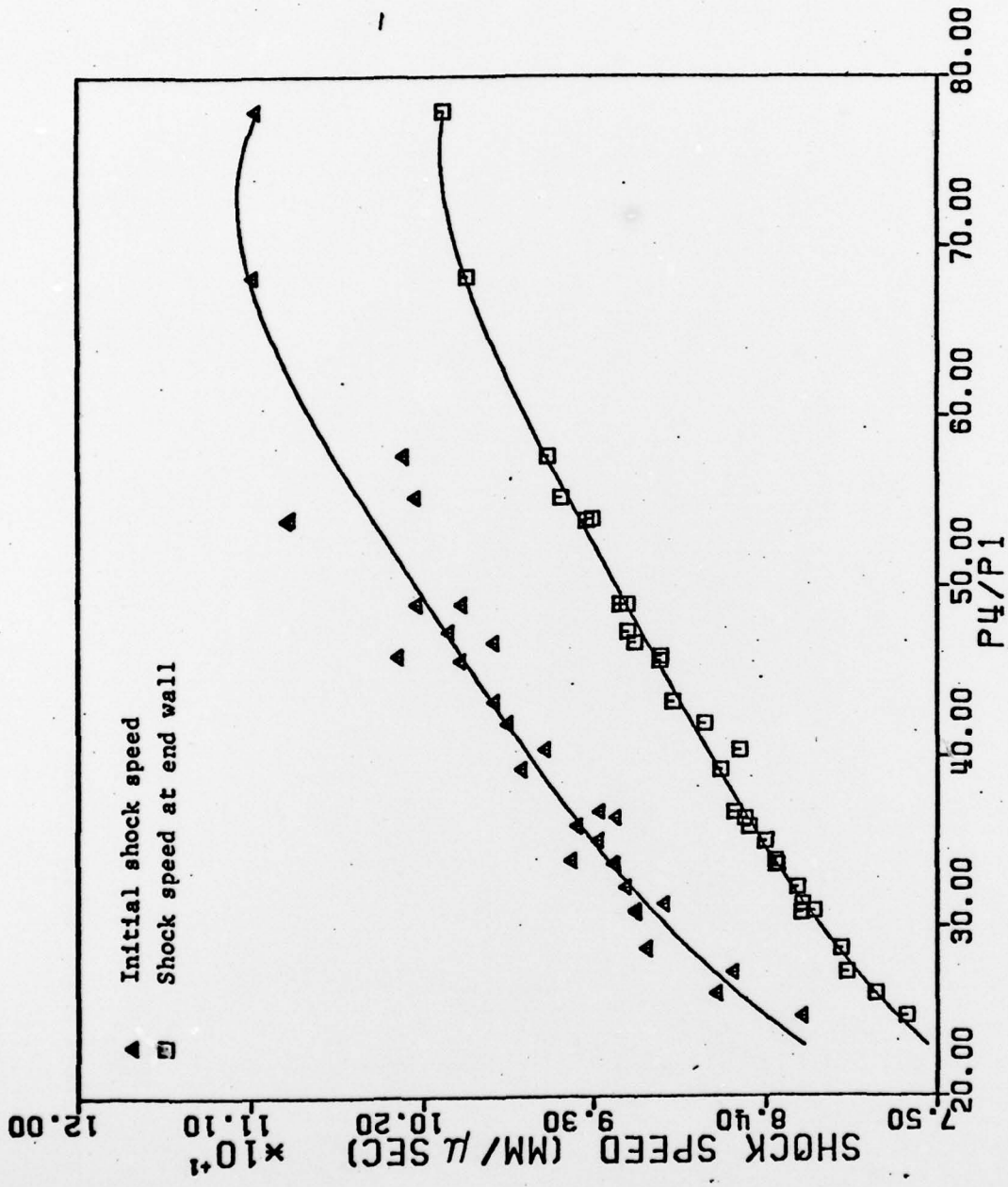

Figure B.3. Calculated initial shock speed and shock speed at end wall as a function of shock strength for a group of typical toluene/argon mixture shocks.

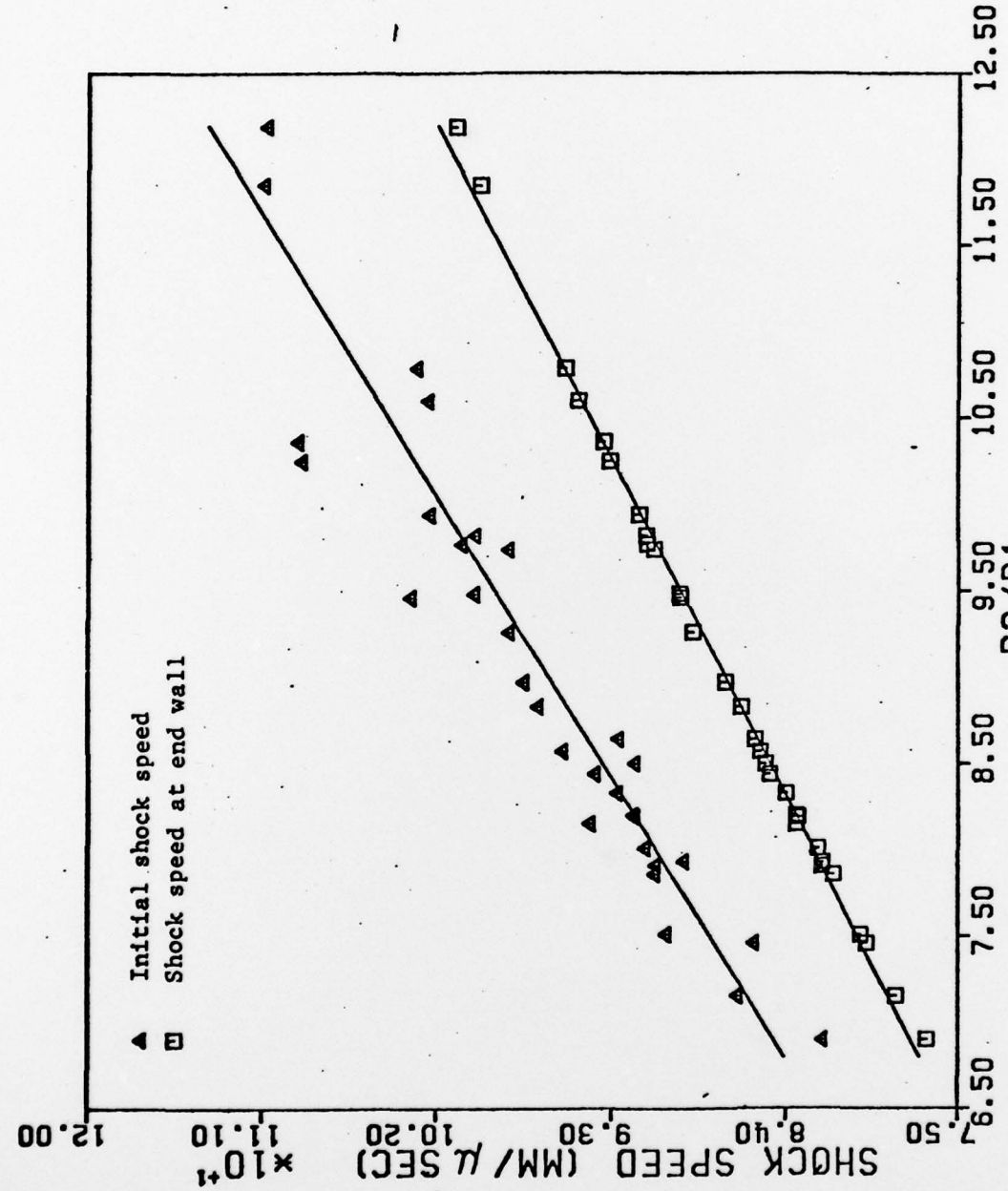

Figure B.4. Calculated initial shock speed and shock speed at end wall as a function of shock strength for a group of typical toluene/argon mixture shocks.

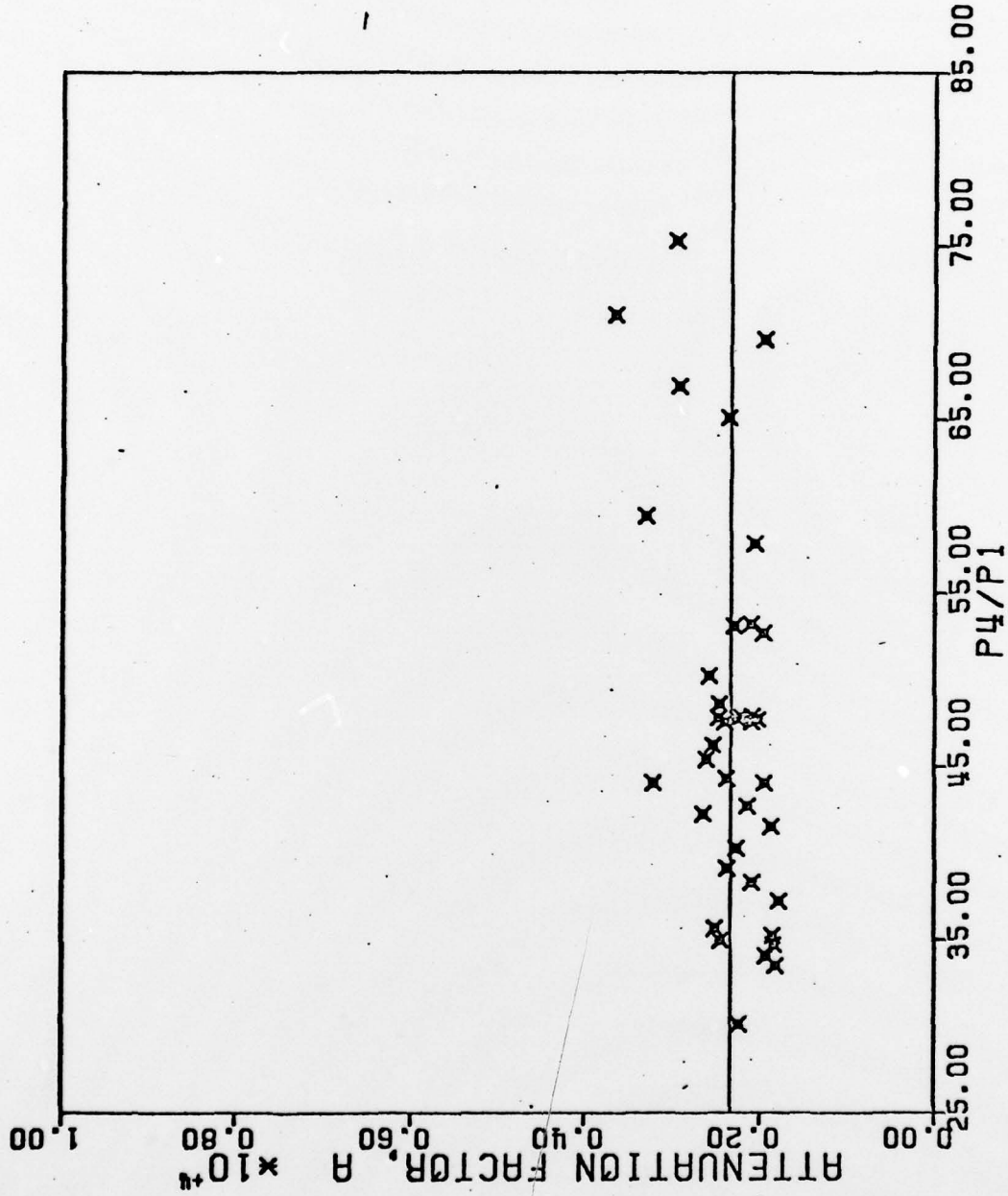

Figure B.5.Calculated attenuation factor as a function of shock strength for a group of typical toluene/argon mixture shocks.

being used, (2) the effect of the filling speed during the pressurization of the driver section, (3) the inconsistency of the opening time of the primary diaphragm which arises from the speed of venting the spacer. In our experiments, we do find the averaged attenuation factor in three inch diameter shock tube is less than that in one inch shock tube. Therefore, the attenuation factor should be a strong function of the characteristics of the shock tube, e.g., the shape of the cross section, hydraulic diameter, double or single diaphram mode; and a weak function of the shock strength and the composition of the test gas.

A linear relationship between the shock speed at end wall and the average speeds for three different intervals is given in Figure B.6. The information reveals the extent of attenuation of the wavespeed per increment of the distance traveled is approximately the same. Generally speaking, for shock strength ranging from 25 to 80, the extent of attenuation is less than 1.5% per meter.

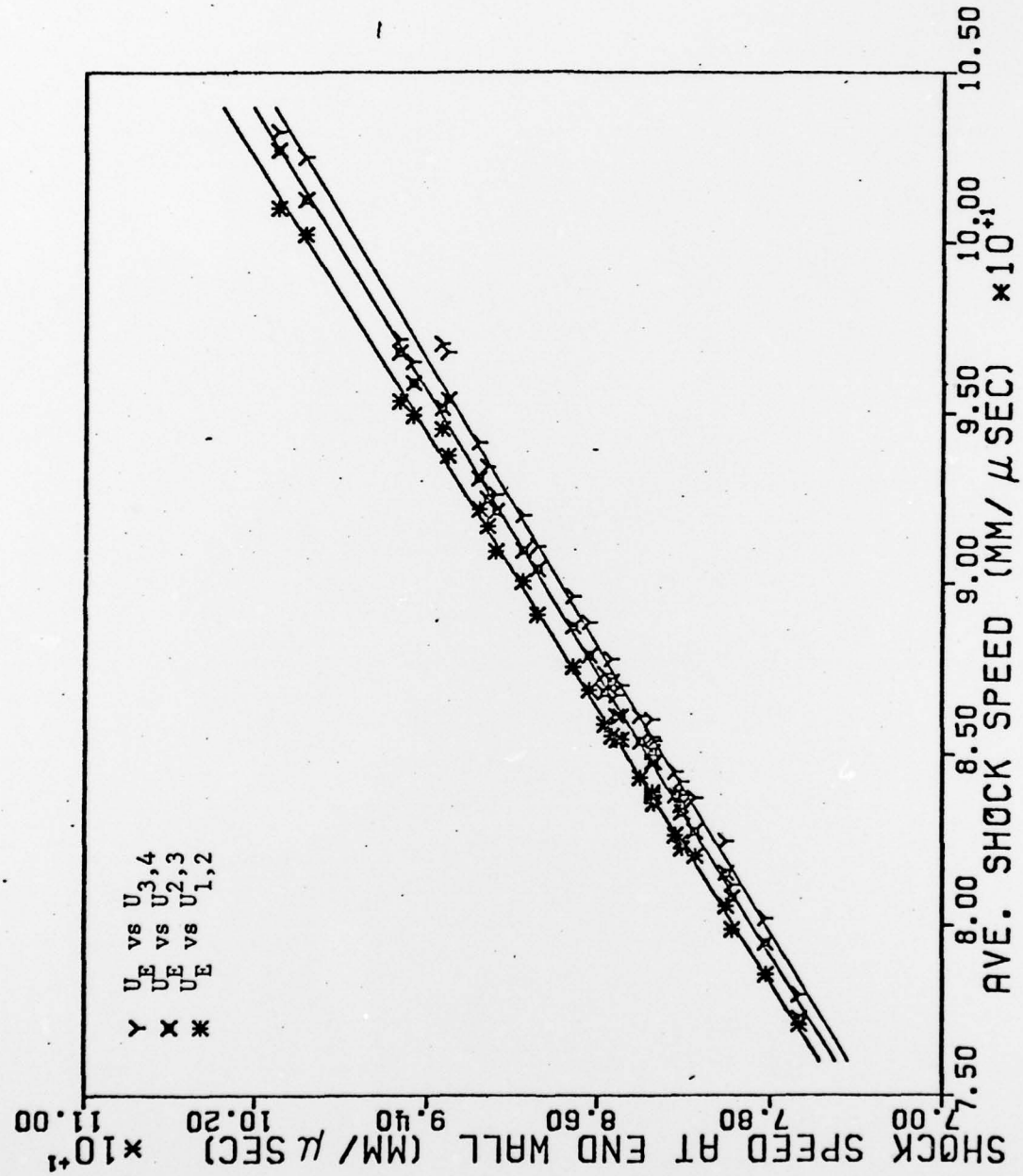

Figure B.6.Calculated shock speed at end wall as a function of average shock speed measured from three different intervals.

REFERENCES

1. Matula, R. A. and R. C. Farmer, "Combustion Kinetics of Selected Aromatic Hydrocarbons", AFOSR-TR-78-1294, June, 1978.

2. Smith, R. D., "A Direct Mass Spectroscopic Study of the Mechanism of Toluene Pyrolysis at High Temperatures", J. Phys. Chem., 83, pp. 1554-1563, 1979.

3. Miller, W. J. and H. F. Calcote, "Fundamental Mechanisms of Carbon Formation in Hydrocarbon and Synthetic Fuel Combustion", in Abstracts 1978 AFOSR Contractors Meeting on Air-Breathing Combustion Dynamics, AFOSR TR-78-1255, Oct. 1978.

4. Fujii, N. and T. Asaba, 14th Symp. (International) Comb., p. 433, 1973.

5. Kogarko, S. M. and A. A. Borisov, Bull. Acad. Sci., USSR, No. 8, 1255. (1960).

6. Miyama, H., "Initiation of Aromatic Hydrocarbon - Oxygen Mixtures by Shock Waves", J. Phys. Chem., 75, pp. 1501-1504, 1971.

7. Baker, J. A., G. B. Skinner, Comb. and Flame, Vol. 19, 247-350 (1972).

8. Chakraborty, B. B., and Long, R., "The Formation of Soot and Polycylic Aromatic Hydrocarbons in Diffusion Flames III; Effect of Additions of Oxygen to Ethylene and Ethane Respectively as Fuels, "Comb. & Flame, 12, pp. 469-476, 1968.

9. Homann, K. H., "Carbon Formation in Premixed Flames", Comb. & Flame, Vol. 11, pp. 265-287, 1967.

10. Clarke, A. E., Hunter, T. G., and Garner, F. H., "The Tendency to Smoke of Organic Substances on Burning", J. Inst. Pet., 32, pp. 627-642, 1946.

11. MacFarlene, J. J., Hoderness, F. H., and Whiteher, F. S. E., "Soot Formation Rates in Premixed C_5 and C_6 Hydrocarbon-Air Flames at Pressure up to 20 Atmospheres", Comb. & Flame, 8, pp. 215-229, 1964.

12. Schala, R. L., and Hibbard, R. R., "Smoke and Coke Formation in the Combustion of Hydrocarbon-Air Mixtures", Chapter IX in "Basic Considerations in the Combustion of Hydrocarbon Fuels with Air", NACA Report 1300, pp. 242-255, 1957.

13. Street, J. C., and Thomas, A., "Soot Formation in Premixed Flames", Fuel, 34, pp. 4-36, 1955.

14. Fennimore, C. P., Jones, G. W., and Moore, G. E., "Carbon Formation in Quenched Flat Flames at 1600°K", 6th Symp. (International), Comb., pp. 242-246, 1956.

15. D'Alessio, A., DiLorenzo, A., Sarofim, A. F., Beretta, F., Masi, Jr., and Venitozzi, C., "Soot Formation in CH_4-O_2 Flames," 15th Symp. (International) Comb., pp. 1417-1438, 1974.

16. Palmer, H. B., and Cullis, C. F., "The Formation of Carbon From Gases", Chemistry & Physics of Carbon, edited by P. L. Walker, 1965.

17. Wagner, H. Gg., "Soot Formation in Combustion", Plenary Lecture 17th Symp. (International) Comb., 1978.

18. Flobdrof, J. Wagner, H. Gg., Z. Phys. Chem. NF 54, 8, 1967.

19. Wright, F. J., "Carbon Formation Under Well-Stirred Conditions, Part II", Comb. & Flame, 15, pp. 217-222, 1970.

20. Wright, F. J., "The Formation of Carbon Under Well-Stirred Conditions" 12th Symp. (International) Comb., p. 867, 1967.

21. Radcliff, S. W., Appleton, J. P., "Shock-Tube Measurements of Carbon to Oxygen Atom Ratios for Incipiant Soot Formation with C_2H_2, C_2H_4 and C_2H_6 Fuels", Comb. Sci. & Tech., 3, pp. 255-262, 1971.

22. Baulch, D. L., Drysdale, D. D., Hourne, D. G. Lloyd, A. C., Elevated Kinetic Data for High Temperature Reactions, 3, Leeds, 1972.

23. Gaydon, A. G., and H. G. Wofhard, Flames, 2nd ed., Chapman and Hall, London, 1960.

24. Mie, G., Ann. Physik, 25, 377, 1908.

25. Lower, T. M., and A. J. Newall, "The Emissivities of Flame Soot Dispersions", Comb. & Flame, 16, pp. 191-194, 1971.

26. Foster, P. J., "Calculation of the Optical Properties of Dispersed Phases", Comb. & Flame, 7, No. 3, pp. 277-282, 1963.

27. Voorhies, A., Jr., "Petroleum Refining Technology", Class Notes, ChE Dept., LSU, Baton Rouge, LA, May 1978.

28. Stein, S. E., "On the High Temperature Chemical Equilibrium of Polycyclic Aromatic Hydrocarbons", J. Phys. Chem., 82, 1978.

29. Stein, S. E., D. M. Golden and S. W. Benson, "Predictive Scheme for Thermochemical Properties of Polycyclic Aromatic Hydrocarbons", J. Phys. Chem., 81, No. 4, 1977.

30. Burcat, Alexander, Personal Communication.

31. Sanderson, T. R., Chemical Bonds in Organic Compounds, Sun and Sand Publishing Co., 1976.

32. Santoro, R. and I. Glassman, "A Review of Oxidation of Aromatic Hydrocarbons", Comb. Sci. & Tech., 19, pp. 161-164, 1979.

33. Golden, M., "Pyrolysis & Oxidation of Aromatic Compounds"- NBS Alternative Fuel Meeting, Washington, D.C., 1977.

34. Keating, E. L., "High Temperature Decomposition and Oxidation of C_2F_4", Ph.D. Thesis, Drexel University, Philadelphia, PA, 1973.

35. Milks, D., Ph.D. dissertation, Drexel University, Philadelphia, PA, 1975.

36. Emirch, R. J., and Donald B. Wheeler, Jr., "Wall Effect in Shock Tube Flow" The Physics of Fluids, Vol. 1, No. 1, pp. 14-25, 1958.

37. Berhardt, H. J., "Trajectories of Shock wave and Contact Surface in Real Shock Tube Flow", Project Squid, Contract N00014-67-A-0226-0005, NR-098-038.

38. Albrechcinski, T. M., "Shock tube - diagonstic techniques for the measurement of the radiative flux from strong shock waves in nitrogen", Master thesis, State University of New York at Buffalo, 1975.

39. Kuster, J. L., and J. H. Mize, Optimization Techniques with Fortran, McGraw-Hill Books Company, 1973.